

Review

Research Progress on Atomically Dispersed Fe-N-C Catalysts for the Oxygen Reduction Reaction

Yuebin Lian ^{1,*} , Jinnan Xu ², Wangkai Zhou ², Yao Lin ³ and Jirong Bai ^{3,*} ¹ School of Optoelectronic Engineering, Changzhou Institute of Technology, Changzhou 213032, China² School of Chemistry and Environmental Engineering, Jiangsu University of Technology, Changzhou 213001, China; jinnan_xu@126.com (J.X.)³ Research Center of Secondary Resources and Environment, School of Chemical Engineering and Materials, Changzhou Institute of Technology, Changzhou 213022, China; xiaoduovozz@163.com

* Correspondence: lianyb@czu.cn (Y.L.); baijr@czu.cn (J.B.)

Abstract: The efficiency and performance of proton exchange membrane fuel cells (PEMFCs) are primarily influenced by ORR electrocatalysts. In recent years, atomically dispersed metal–nitrogen–carbon (M-N-C) catalysts have gained significant attention due to their high active center density, high atomic utilization, and high activity. These catalysts are now considered the preferred alternative to traditional noble metal electrocatalysts. The unique properties of M-N-C catalysts are anticipated to enhance the energy conversion efficiency and lower the manufacturing cost of the entire system, thereby facilitating the commercialization and widespread application of fuel cell technology. This article initially delves into the origin of performance and degradation mechanisms of Fe-N-C catalysts from both experimental and theoretical perspectives. Building on this foundation, the focus shifts to strategies aimed at enhancing the activity and durability of atomically dispersed Fe-N-C catalysts. These strategies encompass the use of bimetallic atoms, atomic clusters, heteroatoms (B, S, and P), and morphology regulation to optimize catalytic active sites. This article concludes by detailing the current challenges and future prospects of atomically dispersed Fe-N-C catalysts.



Citation: Lian, Y.; Xu, J.; Zhou, W.; Lin, Y.; Bai, J. Research Progress on Atomically Dispersed Fe-N-C Catalysts for the Oxygen Reduction Reaction. *Molecules* **2024**, *29*, 771. <https://doi.org/10.3390/molecules29040771>

Academic Editors: Isidro M. Pastor and Luísa Margarida Martins

Received: 9 January 2024

Revised: 31 January 2024

Accepted: 5 February 2024

Published: 7 February 2024



Copyright: © 2024 by the authors. Licensee MDPI, Basel, Switzerland. This article is an open access article distributed under the terms and conditions of the Creative Commons Attribution (CC BY) license (<https://creativecommons.org/licenses/by/4.0/>).

1. Introduction

Escalating energy demand and mounting environmental concerns have underscored the importance of developing clean energy conversion technologies. Among these, fuel cells (FCs) and metal–air batteries (MABs) are emerging as vital sustainable and clean energy conversion technologies [1–5]. However, the efficiency of these technologies is often hampered by the kinetics of the oxygen reduction reaction (ORR), a crucial component of energy conversion. This results in high overpotential, low energy efficiency, low power density, and poor cyclic stability of catalytic reactions. Currently, the most effective ORR catalysts are based on precious metals such as platinum (Pt) and its alloys. However, the rising cost of these materials, particularly in the context of proton exchange membrane fuel cells (PEMFCs), has posed significant challenges to their large-scale practical applications [6–9]. Despite the ability of Pt-based catalysts to optimize the performance of air electrodes in fuel cells, their prohibitive cost and dwindling resources have impeded the commercialization of zinc–air batteries (ZABs) and fuel cells. Therefore, the development of more stable, efficient, and cost-effective ORR electrocatalysts is pivotal for the widespread adoption of these energy conversion devices [10–13].

Among the various non-precious metal catalysts proposed as alternatives to precious metal catalysts, atomically dispersed M-N-C catalysts (including Fe, Mn, and Co) have demonstrated promising activity and stability for ORR. This is attributed to their unique electronic structure [3,14–17]. These atomically dispersed catalysts can maximize atom

utilization, use metal resources rationally, and enhance the efficiency of the atom economy. The active centers of these catalysts are derived from their unsaturated coordination environment and distinct electronic structure. Furthermore, the superior atomic dispersion of the catalyst allows it to mimic the electronic interactions and spatial effects of the substrate, thereby boosting its catalytic performance. With their remarkable atomic utilization efficiency and exceptional electrocatalytic activity, atomically dispersed catalysts hold the potential to enhance the electrocatalytic kinetics of ORR [18–20].

M-N-C single-atom catalysts (SACs) need to be extremely small to achieve a high performance, making the enhancement and utilization of metal sites a primary task for improving ORR activity and stability. Atomically precise electrocatalysts, including single atom, diatomic, and clustered polyatomic electrocatalysts, have garnered considerable attention in recent years. Among these, iron-based atomically dispersed ORR electrocatalysts have been the subject of extensive research [21,22]. Experimental results and theoretical calculations have demonstrated that Fe-Nx-structured activated carbon catalysts outperform transition metal-based activated carbon catalysts such as Co, Ni, and Mn in terms of oxygen reduction activity. They exhibit excellent oxygen reduction performance with four-electron selectivity. As a result, atomically dispersed Fe-N-C, with its suitable adsorption/desorption capacity for oxygen-containing species in the catalytic process, is considered to be the most promising non-precious metal electrocatalyst to replace platinum-based materials [23–25]. Furthermore, the Fe-Nx structure not only exhibits a lower kinetic barrier due to the reduction in free energy from O^* to OOH^* , but the robust bonding between the Fe and N atoms also contributes to its superior catalytic stability.

Despite significant breakthroughs in the catalytic activity of Fe and N co-doped carbon-based ORR electrocatalysts, their direct application to the cathode of PEMFCs is still challenged by poor stability and serious durability issues. These issues are mainly due to the degradation of the catalyst layer, partial Fe deactivation, and carbon corrosion, which lead to the loss of active sites and proton transfer performance, thereby affecting the overall activity and stability. This hinders their practical application. Therefore, understanding and analyzing the degradation mechanism of carbon-based catalysts in PEMFCs and identifying effective strategies to improve their stability/durability are of great theoretical and practical value. This paper reviews the common strategies and methods for improving the stability and activity of Fe-N-C catalysts, based on the investigation of their activity origin and degradation mechanism, and discusses the existing challenges.

2. Mechanism Investigation

2.1. General ORR Mechanism

The intrinsic ORR activity of the Fe-N₄ site is linked to the electronic structure of carbon supports. By controlling the electronic structure of these supports, the interaction between the supports and Fe-N₄ site can be altered, leading to changes in the activity of the Fe-N₄ site. However, the essence of this change in Fe-N₄ ORR activity remains a mystery due to the complex factors influencing it. To comprehend the Fe-N₄ ORR activity, numerous attempts have been made to identify the descriptors of Fe-N₄ ORR activity. For instance, the full width at the half-maximum of C 1s photoemission spectra [26], d-band center [27], and the electronegativity of the nearest neighbor atoms [28] are considered to describe the ORR activity of the Fe-N₄ site. However, these descriptors struggle to explain the orientation-dependence and differences in ORR activity at the same Fe-N₄ site on different carbon supports. Liu and his team have proposed a model to understand the ORR activity of the Fe-N₄ site, which is based on the spatial structure and energy level of the frontier orbitals, as determined by density functional theory calculations. Using the regulation of divacancy defects on the Fe-N₄ site's ORR activity as an example, they demonstrate that the hybridization between Fe 3dz², 3dyz (3dxz) and O₂ π* orbitals is the origin of Fe-N₄ ORR activity. Their team discovered that descriptors such as the Fe-O bond length, the d-band center gap of spin states, the magnetic moment of the Fe site, and *O₂ can accurately predict the ORR activity of the Fe-N₄ site. Moreover, these descriptors and the ORR activity

of the Fe-N₄ site are primarily distributed in two regions, with significant differences that are strongly related to the height of the Fe 3d projected orbital in the Z direction [29].

2.2. Origin of Activity

Atomically dispersed Fe-N-C catalysts are among the most active non-precious-metal catalysts for the ORR. These catalysts are primarily synthesized through thermal decomposition. However, the process of converting Fe, N, and C precursors into Fe-N_x active sites during thermal decomposition is not fully understood. This gap in understanding complicates the establishment of an accurate relationship between synthesis conditions and active site structures. Consequently, the true catalytic active sites remain a topic of debate. This uncertainty has led to the reliance on trial and error and enumeration methods for improving activity and stability in experimental processes, significantly hindering the practical application of atomic Fe-N-C catalysts.

Research indicates that the adsorption of Fe³⁺ leads to the formation of FeO_x particles. These particles transform into atomically dispersed Fe-N₄ coordination structures during thermal activation, which increases the density of Fe-N₄ active centers. This transformation is primarily due to the higher thermal stability of Fe-N₄ structures compared to FeO_x. Various factors, including coordination number, symmetry, and changes in the length of the Fe-N bonds in the Fe-N_x coordination structure, can alter the charge distribution of the central Fe ion and the surrounding C atoms. These alterations influence the adsorption of O₂ on the Fe-N₄ site and the cleavage of O-O bonds, ultimately determining the performance of the catalyst [30]. Deborah J. Myers and her team conducted an in-depth study on the changes in the geometric and electronic configuration of the active center Fe atom during *in situ* high-temperature pyrolysis using X-ray absorption spectroscopy (Figure 1) [31]. Their findings shed light on the complex process of converting the precursors to the Fe-N_x active sites during high-temperature pyrolysis. The team discovered that the Fe precursor transforms into Fe oxide below 300 °C. Subsequently, a tetrahedral Fe₁(II)-O₄ structure forms through a crystal-melt transition below 600 °C. Importantly, above 600 °C, Fe₁(II)-O₄ releases a single Fe atom, leading to the formation of Fe₁(II)-N₄ active sites. Based on these insights, the authors suggest a novel non-contact pyrolysis method. In this method, the metal and the nitrogen-doped carbon (N-C) substrate do not have direct physical contact. At high temperatures, gaseous metal atoms are captured by nitrogen defects through gas-phase metal single-atom migration mechanisms, forming active sites.

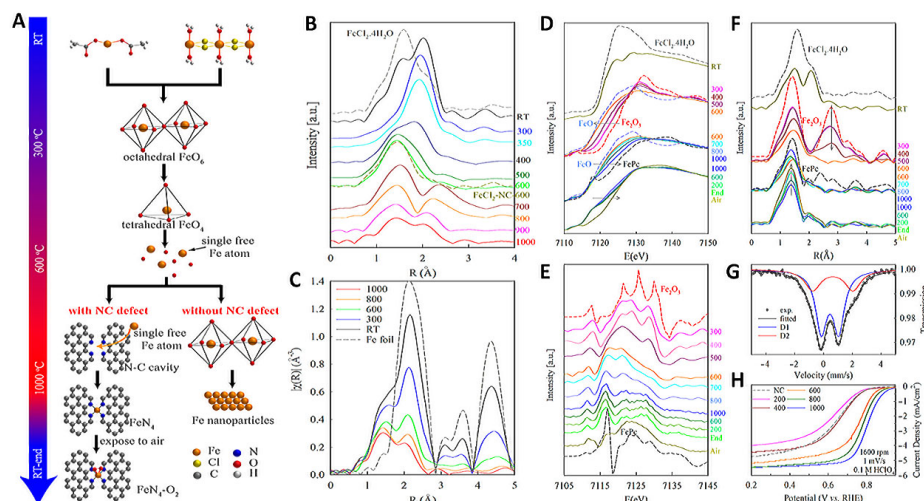


Figure 1. (A) Schematic illustration of the thermal evolution of iron compounds up to 600 °C. (B,C) Fourier transform extended X-ray absorption fine structure (FT-EXAFS) spectra. (D) X-ray absorption near edge structure (XANES). (E) Fourier transform (FT)-EXAFS. (F) The first derivative of the XANES spectra. (G) A 57Fe Mössbauer spectrum. (H) Rotating disk electrode (RDE) polarization plots of FeCl₂-NC-T catalysts [31]. Copyright © 2023 American Chemical Society.

Zhou and his team conducted an extensive investigation of 13 different ortho-ligand FeN_xC conformations and their corresponding ORR activities. They simulated a realistic electrocatalytic environment using a constant potential implicit solvent model (Figure 2A,B) [32]. The study clarified the mechanism of how different types of ligand nitrogens (pyridine and pyrrole nitrogen) and pH influence the ORR catalytic activity. The findings revealed that pyrrolic nitrogen enhances the ORR activity more effectively than the ligand pyridine nitrogen. Among the configurations studied, FeN_4C containing pyrrolic nitrogen exhibited the highest activity in an acidic medium. Moreover, the high ORR performance of Fe-N-C in alkaline electrolytes was attributed to the in situ conversion of the active center to $^*\text{O}-\text{FeN}_4\text{C}$ and $^*\text{OH}-\text{FeN}_4\text{C}$. Liu et al. investigated the energy levels of the frontier orbitals and the spatial structure to elucidate the origin of the activity of the Fe-N₄ sites through density functional theory (DFT) calculations, and the origin and correlation of these descriptors were summarized (Figure 2D–I) [29]. The results show that the Fe-O bond length ($L_{\text{Fe}-\text{O}}$) can accurately describe the ORR activity of the Fe-N₄ site. From the electronic configuration point of view, the spin state of the magnetic moment of the Fe site, the d-band center gap, and $^*\text{O}_2$ are almost linearly related to the ORR activity of the Fe-N₄ sites.

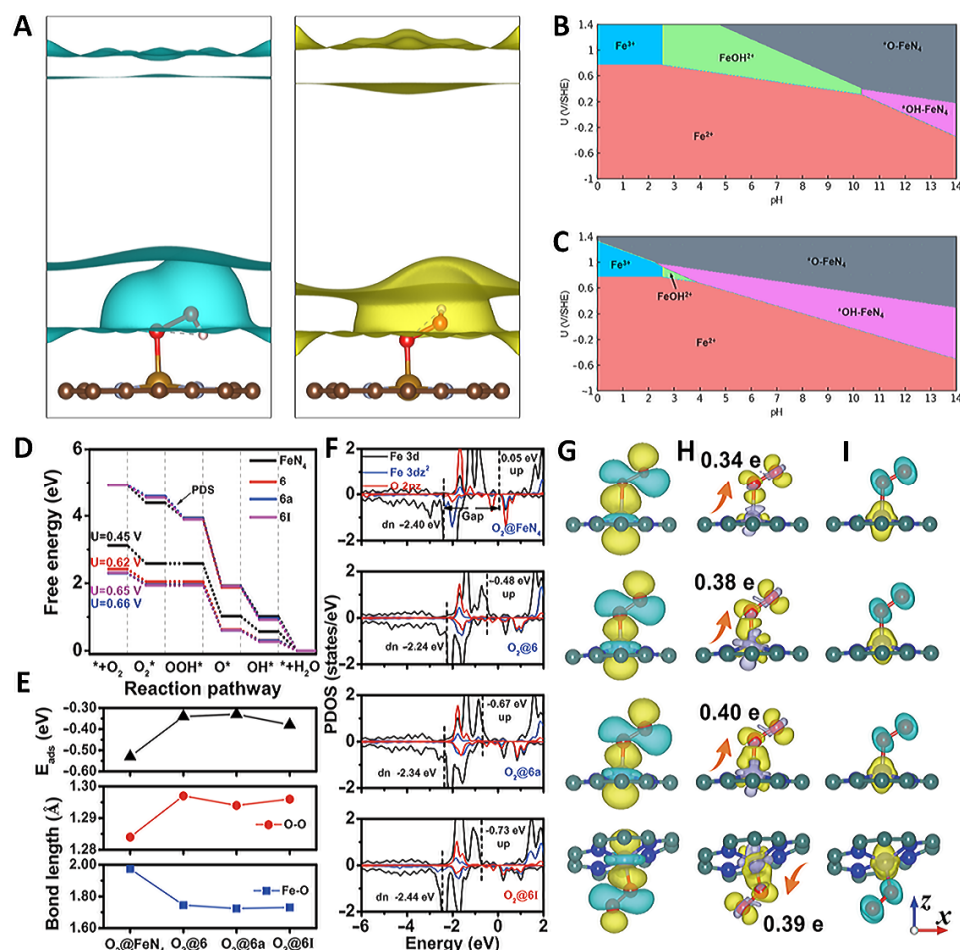


Figure 2. (A) Ionic countercharge density for $^*\text{OOH}$ corresponding to -2.01 V/SHE and 1.88 V/SHE . Stability diagram of the (B) pyridinic FeN_4C slab and (C) pyrrolic FeN_4C slab [32]. Copyright © 2023 American Chemical Society. (D) Gibbs free energy diagrams, (E) adsorption energy, (F) PDOS, (G) maximally localized Wannier functions of $\text{Fe} 3d_z^2$, $\text{O}_2 2p_z$ orbital, (H) charge density difference, (I) spin density [29]. Copyright © 2023 Springer Nature.

2.3. Degradation Mechanism

Atomically dispersed Fe-N-C catalysts, due to their efficient atomic utilization and remarkable catalytic activity, are considered to be the most promising alternatives to platinum group metal (PGM) electrocatalysts. However, optimizing the performance of Fe-N-C presents a significant challenge due to a trade-off between stability and activity. Their stability in PEMFCs is not satisfactory, leading to rapid performance degradation. Currently, the degradation mechanism of Fe-N-C in PEMFCs is not well understood, and the complex phenomena and difficulties in understanding the mechanisms of Fe-N-C cathode deactivation hinder the development of solutions to enhance stability. There is a lack of in-depth electrochemical in situ analysis. The degradation mechanism of M-N-C SACs primarily involves protonation of N active sites, oxidation of free radicals on the catalyst, and detachment of metal species from the active site. The main cause of performance degradation of Fe-N-C SACs in PEMFCs is Fe demetallation and carbon corrosion. Fe-N_x sites in Fe-N-C catalysts undergo metal detachment, resulting in the loss of active sites. Simultaneously, carbon substrates in the catalyst layer undergo corrosion, reducing the ORR rate around the active sites [33–35].

Zhao et al. employed advanced electrochemical analysis methods to investigate the rapid degradation phenomenon and unveiled the complexity of these degradation mechanisms through cyclic voltammetry and relaxation time distribution analysis (Figure 3A–E) [36]. After operating a practical proton exchange membrane fuel cell (PEMFC) with an Fe-N-C catalyst for 60 h, they discovered that up to 75% of the active sites in the catalyst layer were deactivated due to iron demetallation. The amount of carbon corrosion material in the catalyst layer increased fivefold, the proton transfer kinetics decreased fourfold, and the pathways for gas, ions, and electrons to the catalytic sites were extended, resulting in a threefold decrease in the ORR rate.

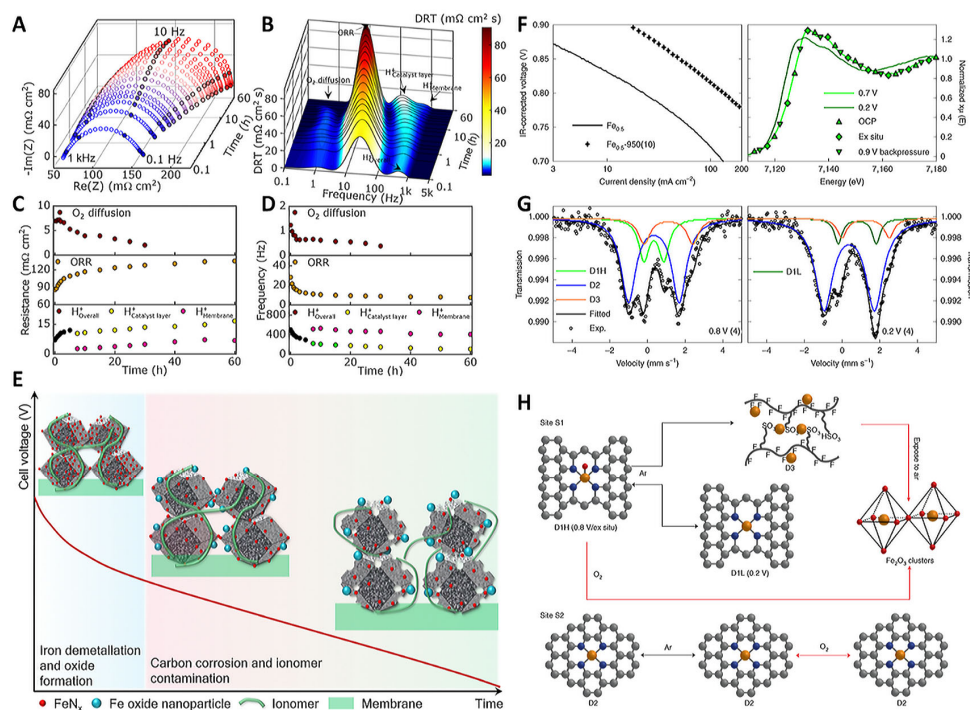


Figure 3. (A) Nyquist plot. (B) DRT plot. (C) Resistance and (D) characteristic frequencies. (E) Degradation mechanism of Fe-N-C at different reaction stages [36]. Copyright © 2023 The Royal Society of Chemistry. (F) Tafel plots and Fe K-edge XANES spectra, (G) in situ ⁵⁷Fe Mössbauer spectra. (H) Structural changes [37]. Copyright © 2020 Springer Nature.

Frédéric Jaouen et al. conducted a study on Fe-N-C electrocatalysts with more stable Fe-N_x sites and fewer non-durable FeN_x sites using in situ spectroscopy, ex situ spec-

troscopy, and end-of-test spectrum analysis (Figure 3F,G) [37]. Their *in situ* ^{57}Fe Mössbauer spectroscopy analysis revealed that Fe-N-C SACs contain two types of $\text{Fe}-\text{N}_x$ sites, which have similar isomer shifts. Although these sites are common in Fe-N-C, their respective activities and lifetimes are not well understood. The researchers demonstrated that some S1 sites are stable using *in situ* ^{57}Fe Mössbauer spectroscopy in an anoxic PEMFC, and they reversibly transform from high-spin iron to high-spin ferrous iron. Meanwhile, the electronic state of S2 is potential independent and is low- or intermediate-spin ferrous iron (Figure 3H). Chang Hyuck Choi et al. systematically investigated the changes in Fe-N-C active site density and conversion frequency over time under temperature/gas-controlled gas diffusion electrode conditions (Figure 4) [38]. Their results showed that the diagnosis of iron leaching identified a strong dependence of the *in situ* density changes on the operating parameters and plotted the stability over the lifetime. The changes in the main degradation mechanisms during operation were successfully revealed. The researchers also developed a proof-of-concept strategy using separated Pt ions as a non-catalytic stabilizer to improve fuel cell stability by reducing iron dissolution.

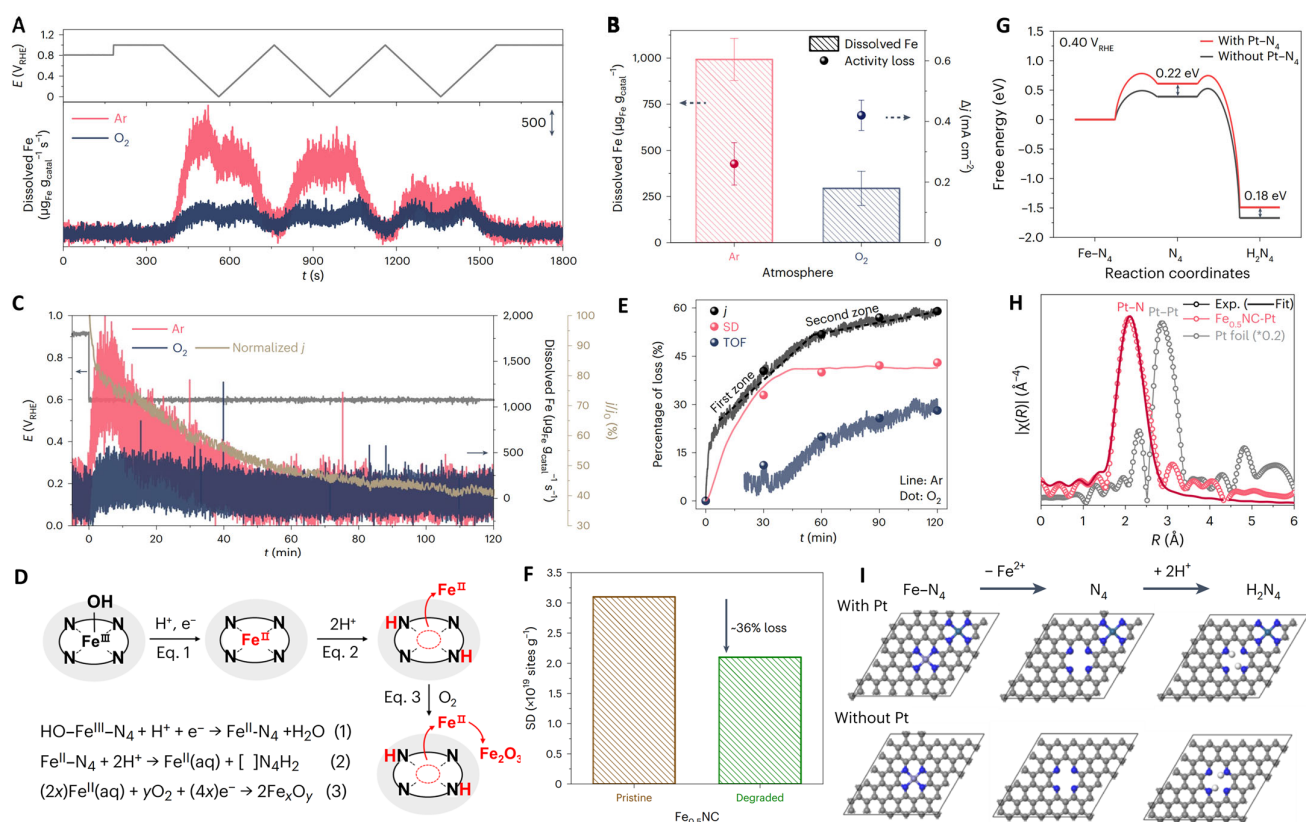


Figure 4. (A) Real-time Fe dissolution of $\text{Fe}_{0.5}\text{NC}/\text{GDE}$. (B) ORR activity loss and Cumulative amounts of dissolved Fe. (C) Real-time Fe dissolution of $\text{Fe}_{0.5}\text{NC}/\text{GDE}$ (at 0.6 VRHE). (D) Proposed mechanism for Fe demetallation. (E) Relative loss of TOF, SD, and j values. (F) Site density value of pristine and degraded $\text{Fe}_{0.5}\text{NC}$. (G) Free energy profiles of the Fe dissolution process. (H) Pt L3-edge FT-EXAFS spectra. (I) DFT-optimized structures [38]. Copyright © 2023 Springer Nature.

2.4. Resistance to Poisoning

In fuel cells, oxygen often unavoidably mixes with small organic molecules (SOMs). As a result, an important aspect of high-performance ORR catalysts is their excellent resistance to SOM poisoning. Many SOMs are easily adsorbed on the surface of Pt and oxidized, which reduces the ORR catalytic activity of the active site. Consequently, current commercial Pt/C catalysts often exhibit poor resistance to SOMs [39]. Fe-N-C catalysts are widely believed to have excellent resistance to SOM poisoning. However, a study by Sun's group showed that methanol and ethanol significantly inhibited the ORR process of Fe-N-C

catalysts rich in micropores (PDA-Fe-N-C) in an alkaline environment. The investigation of the size, polarity, and inhibition ability of organic molecules revealed that SOMs with a low polarity and larger size had a more pronounced inhibitory effect on the catalyst performance. The inhibition is believed to be due to the filling of the micropores by the SOMs, leading to a decrease in the mass transfer capacity. Interestingly, this suppression phenomenon did not occur in an acidic environment. This could be attributed to the protonation of the N group, which changes the polarity of the micropores and reduces the adsorption of SOMs [40].

3. Performance Improvement Strategy

3.1. Heterogeneous Atom Doping

Heteroatom doping can induce lattice distortions in electronic density, thereby activating catalytic active sites in the material. This typically introduces intermediate electronic states that act as a bridge to lower the charge transfer energy barrier between the catalyst and the surface adsorbate. Dopants can modify the electronic energy levels and local electronic distribution around them, making them active sites for catalytic reactions. Doping carbon with one or more active atoms can effectively optimize the bonding and antibonding states by adjusting the energy levels of the valence orbitals. The introduction of active atoms increases the energy of the active orbital and reduces the occupation of the antibonding state, which can optimize the adsorption of intermediates and improve the efficiency of the catalytic reaction. This fundamental physical principle is the basis for enhancing the catalytic performance of heteroatom-doped carbon. Theoretical studies have shown that the doping of heteroatoms is particularly attractive for improving ORR performance because they can drive defects into a confined state near the Fermi level [41–57]. The electronegativity and atomic size of P are lower than that of N, so doping P can optimize the spin density and local charge, while doping S in the graphene skeleton can modify the electronic configuration [41,49]. The co-doping of various non-metallic heteroatoms is an effective way to optimize the adsorption of oxygen-containing intermediates, regulate the local coordination environment, and improve the catalytic performance. In particular, co-doping with P can promote the transfer of electrons from C to N and the formation of more active sites, while the presence of S and N can break the uniformity and induce charge redistribution in the carbon skeleton [50–52]. Similarly, hybridization between the sp-orbitals of B and the d-orbitals of the transition metal contributes to the optimized properties of the d-band [53]. The coordination effect of heteroatoms will undoubtedly provide a new opportunity for the study of ORR in the future.

In addition, dopants can activate electron acceptor or electron donor states under different reaction conditions by creating favorable band gaps, electron structures, and state densities. This determines the number of free radicals and the energy consumption of charge transfer. Moreover, the derived active center significantly affects the interactions between reaction intermediates and the reduction in the electrode overpotential. The special configuration of some dopants can provide a durable reaction pathway. Breaking the symmetric electron distribution in the iron center of the single atom is an efficient way to optimize the intrinsic activity of the ORR. S [41–48], P [49–52,54–64], B [53], and other dopants provide an excellent method for enhancing the ORR performance of Fe-N-C. S atoms have a lower electronegativity and a larger atomic radius than N atoms. Therefore, Fe-N₃S formed by S replacing N in Fe-N₄ increases the outermost electrons of Fe atoms, resulting in a lower energy requirement for the ORR process compared to Fe-N₄, effectively improving ORR performance. Tan et al. employed a straightforward template strategy and an advanced pyrolysis route to synthesize the Fe-N₃S-C catalyst [65]. This catalyst exhibited an optimized pore structure and coordination environment, remarkably enhancing the active site density and catalytic performance (Figure 5). It also showed excellent ORR long-term durability and catalytic activity. The introduction of the S atom changes the electronic configuration of Fe-N_x, which helps to improve its intrinsic catalytic activity. The layered mesoporous structure of the Fe-N₃S-C catalyst is conducive to anchoring more

iron atoms and exposing more active sites. Such a strategy could extend the application of traditional Fe-N-C electrocatalysts to more complex rechargeable ZABs.

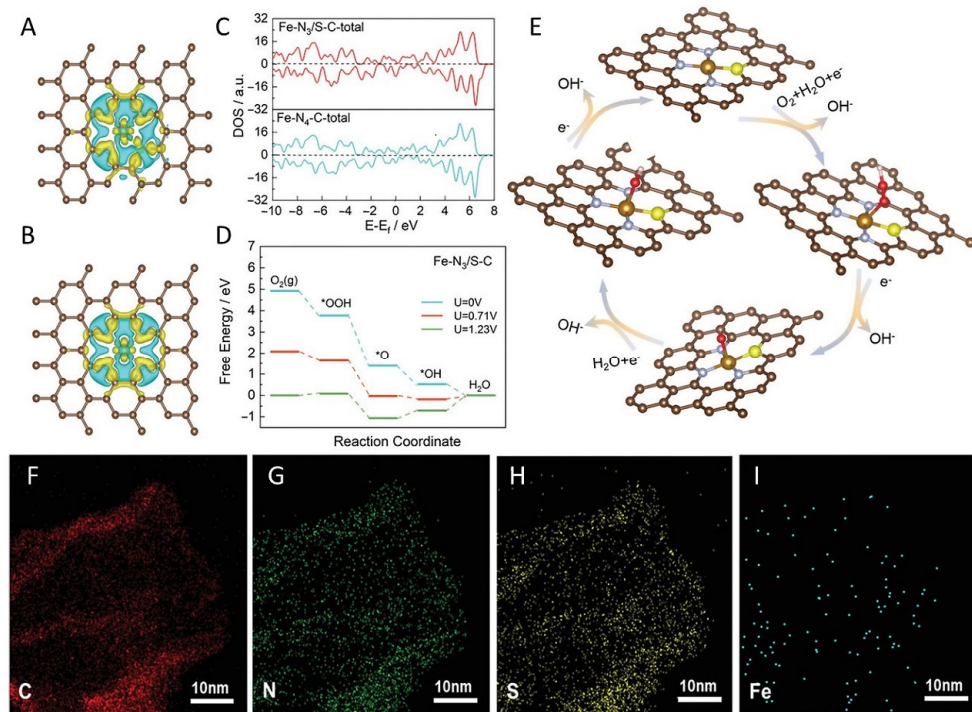


Figure 5. Charge density distribution of (A) $\text{Fe-N}_3/\text{S-C}$ and (B) $\text{Fe-N}_4\text{-C}$. (C) DOS of $\text{Fe-N}_3/\text{S-C}$ and $\text{Fe-N}_4\text{-C}$. (D) Free energy diagram, (E) reaction pathways of $\text{Fe-N}_3/\text{S-C}$; Fe (brown), N (grey), S (yellow). (F–I) STEM image and elemental mapping; C (red), N (green), S (yellow), Fe (blue) [65]. Copyright © 2023 Wiley & Sons.

Compared to N and S doping, P doping in Fe-N-C SACs exhibits a stronger electron-donating ability. Similar to S doping, it can modify the electronic structure of Fe-N-C-based materials, reducing the adsorption energy of the ORR and thereby significantly enhancing the ORR activity. Xue et al. synthesized an atomically dispersed FeN_2P_2 -based material, which demonstrated excellent ORR activity across the entire pH range. The half-wave potentials ($E_{1/2}$) were 0.86 V for acidic electrolytes, 0.83 V for neutral electrolytes, and 0.92 V for alkaline electrolytes (Figure 6A–D) [58]. These are the best-performing catalysts reported to date. Moreover, there was no significant degradation in the performance after 30,000 cycles of durability testing, outperforming commercial Pt/C materials. FeN_2P_2 also exhibited excellent methanol tolerance. More importantly, the FeN_2P_2 -assembled ZABs outperformed the Pt/C-assembled ZABs, indicating the potential of FeN_2P_2 for practical applications. Zong et al. reported an FeN_3P -based material and proposed a strategy to construct iron and phosphorus dual-atom sites to enhance ORR activity and durability. The improved performance of the FeN_3P -based material is attributed to the synergistic effect of the hydrogen bond interaction between the adsorbed and desorbed intermediates composed of neighboring Fe and P atoms (Figure 6E–H) [66]. On the other hand, since the P atom is not directly coordinated with the Fe atomic center, P doping in Fe-N-C helps regulate the electronic density of the Fe-N_4 site, thereby enhancing its ORR performance. Simultaneously, this modified electrocatalyst also exhibits outstanding performance in ZABs and excellent cyclic stability.

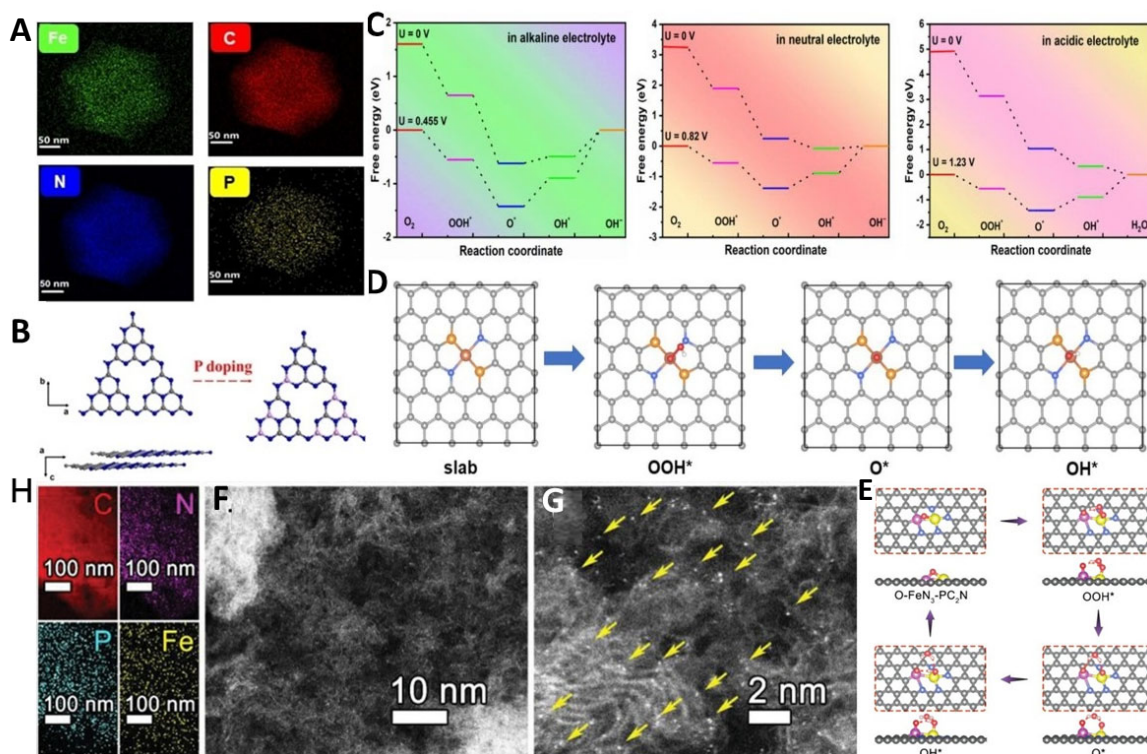


Figure 6. (A) Corresponding EDS results of Fe-SA/PNC. (B) Formation process of P-doped C₃N₄. (C) Gibbs free energy diagrams, (D) possible ORR process of Fe-N₂P₂; Fe (dark brown), N (blue), P (yellow) [57]. Copyright © 2023 Wiley & Sons (E) EDS elemental mapping images, (F,G) HAADF-STEM images of Fe,P-DAS@MPC; arrows (Fe SACs), (H) DFT-optimized adsorption configurations of FeN₃-PC₂N; C (red), N (purple), P (blue), Fe (yellow) [66]. Copyright © 2022 Wiley & Sons.

3.2. Bimetallic Atom

Bimetallic atomic catalysts, composed of two different types of atoms, possess unique catalytic properties and activities. They exhibit a superior catalytic activity, stability, and multi-functionality compared to traditional SACs. By adjusting the interactions between atoms, these catalysts can achieve structural controllability. They are extensively used in ORR, water splitting for hydrogen production, and CO₂ reduction, playing a significant role in energy conversion and environmental protection [67–69]. Through rational design and adjustment, the proportion, structure, and distribution of bimetallic atomic catalysts can be optimized for enhanced catalytic effects. As such, bimetallic atomic catalysts are considered to be the next generation of high-efficiency catalytic materials, with enormous potential in future catalytic research. However, further in-depth research is needed to fully exploit their advantages and overcome existing challenges.

As a unique type of catalytic material, bimetallic atomic catalysts have distinctive performance and application potential in catalytic reactions. With the increasing demands for catalyst activity and selectivity, the research and application of bimetallic atomic catalysts will continue to garner attention, playing a crucial role in energy conversion, environmental protection, and chemical synthesis. Bimetallic catalysts, when compared with monometallic catalysts, display synergistic effects. These effects are a result of metal–metal bonding interactions, which significantly enhance catalytic performance [70,71]. This improvement is demonstrated by DFT calculations, which show that the synergistic effects between bimetals can substantially reduce the reaction activation energy, which achieves the remarkable effect of 1 + 1 > 2 [72]. Bimetallic catalysts, due to their geometric (or strain) effect [73], electronic (or ligand) effect [74], and stabilizing effect [75], demonstrate excellent ORR activity, a high stability, and economic effectiveness [76]. Naiwrit Karmodak and colleagues identified single- and double-atom metal dopants from the first row of transition metals

loaded on the surface of nitrogen-doped graphene containing defects for ORR using a catalyst calculation screening method (Figure 7) [77]. The study identified 4 SACs and 15 double-atom catalysts (DACs) with a high electrocatalytic performance based on the formation energy calculation and microscopic kinetic modeling of the reaction pathway. In the optimal SACs, Mn-N_x exhibits a high durability in both alkaline and acidic media. For the DACs, four potential candidates were identified, namely MnNi, CoCo, FeFe, and MnMn, all of which demonstrated excellent stability over a wide pH range.

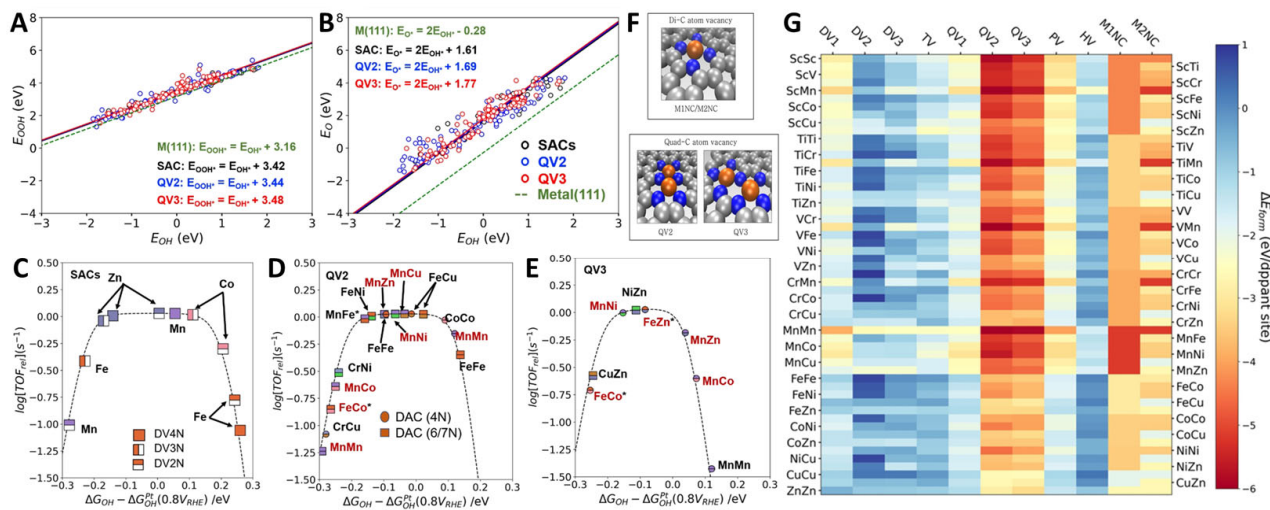


Figure 7. (A,B) Scaling relations of oxygen intermediates. (C–E) ORR activity volcano plots for the DACs and SACs. (F) Di-carbon atom vacancy site; Fe (golden), N (blue), C (grey). (G) Formation energy heat map for the DACs and SACs [77]. Copyright © 2023 Wiley & Sons.

In experimental research, a large number of diatomic electrocatalysts have been reported for the application of ORR. Among these, Fe-based diatomic catalysts mainly include FeMn [78–88], FeCo [89–94], FeCu [95,96], and FeNi [14,97–104]. Zhang et al. reported that doping of Mn atoms in Fe-N-C catalysts improves the ORR performance. The interaction between Mn and Fe is mainly due to the 3d orbitals, and the Mn-N structure in the Fe-Mn-N-C catalyst can effectively activate the neighboring Fe^{III} sites through electronic regulation and the spin state transition (Figure 8) [105]. There is a significant overlap between Mn 3d and Fe 3d, allowing Mn^{II} to capture electrons from Fe^{II}, resulting in a redistribution of electrons in Fe 3d. Moreover, the 3d orbital hybridization of Mn and Fe significantly reduces the energy band gap of Fe,Mn-N-C and numerous effective electron mass and increases the dispersion of the conduction band, thereby optimizing the electronic transport. The Fe,Mn-N-C electrocatalyst shows outstanding ORR performance due to the synergistic effects of Mn and Fe. In particular, it shows excellent durability in ZABs. Density functional theory (DFT) calculations further clarify the reason for the high ORR activity of Fe,Mn-N-C. When oxygen is adsorbed by the Fe-Mn bimetallic atom pair, it creates a suitable bond length, thereby reducing the dissociation energy barrier. Moreover, it can effectively trap oxygen-containing species and rapidly break the bond of M-OH, ensuring the regeneration of OH* and O*. In addition, the enhanced performance of ORR is also attributed to the effective inhibition of peroxide formation.

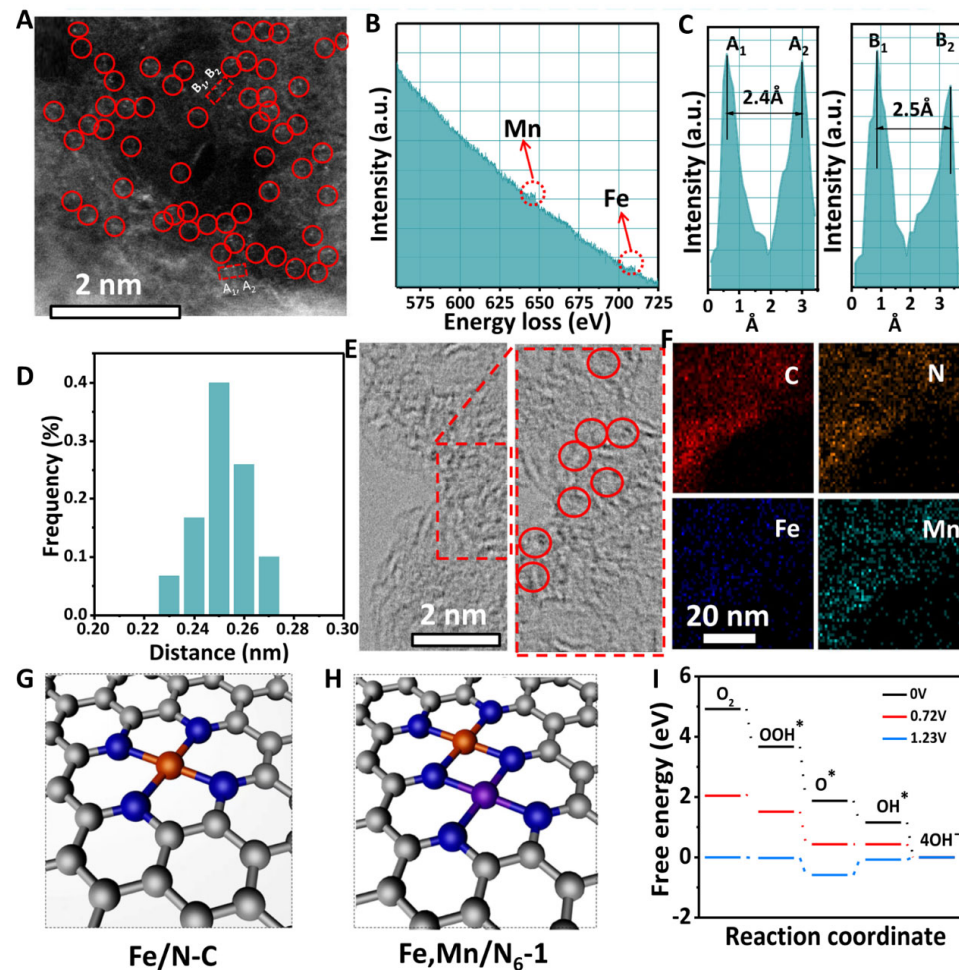


Figure 8. (A) HAADF-STEM image of bimetallic Fe/Mn sites, red circles (bimetallic Fe/Mn sites) (B,C) EELS of Fe-Mn sites. (D) Distance of Fe-Mn diatomic pairs. (E) HRTEM, (F) HAADF-STEM image and element mappings of Fe,Mn/N-C, red circles (bimetallic Fe/Mn sites). Optimized structures of (G) Fe/N-C and (H) Fe,Mn/N-C; Fe (orange) Mn (purple), N (blue), C (grey). (I) Free energy for Fe,Mn/N-C [105]. Copyright © 2021 Springer Nature.

In the volcanic diagram of ORR, Cu, as a non-noble metal, shows a better ORR performance compared to platinum. A significant amount of research has shown that the ORR activity of FeCu-N-C catalysts is superior to that of Fe-N-C SACs in various coordination structures. This is mainly due to the introduction of Cu, which can effectively change the electronic configuration of Fe SACs. Therefore, doping Cu metal atoms in Fe-N-C SACs is an efficient method to optimize their ORR performance. Xiao et al. reported FeCu-N-C DACs containing dual active sites of Fe-N₄ and Cu-N₄. Theoretical calculations were used to determine the Gibbs free energy of the sample's catalyzing ORR [95]. It was found that the rate-determining step (RDS) in the presence of FeN₄ alone is OH → H₂O, as the strong adsorption of FeN₄ on OH hinders the final electron transfer (Figure 9A–E). However, after introducing Cu-N₄, the strain effect caused by the adjacent carbon environment of Cu-N₄ replacing Fe-N₄ attenuated the adsorption ability of the FeN₄-CuN₄ structure on OH, which leads to the RDS of FeCu-NC becoming O → OH, thereby enhancing the catalytic performance and kinetic process. He et al. reported a FeCo bimetallic electrocatalyst which exhibited excellent bifunctional catalytic activity. In addition, its excellent durability during ORR and oxygen evolution reaction (OER) processes was comparable to that of noble metal catalysts (Figure 9F–H) [106]. Calculations showed that the FeCo-N₆ species can serve as the main active sites for both OER and ORR. The performance of FeCo-N-C was improved when compared to conventional single Fe and Co SACs. Moreover, the use of FeCo-N-C

DACs for air cathodes in rechargeable and flexible ZABs resulted in high power density and long-term cycling durability.

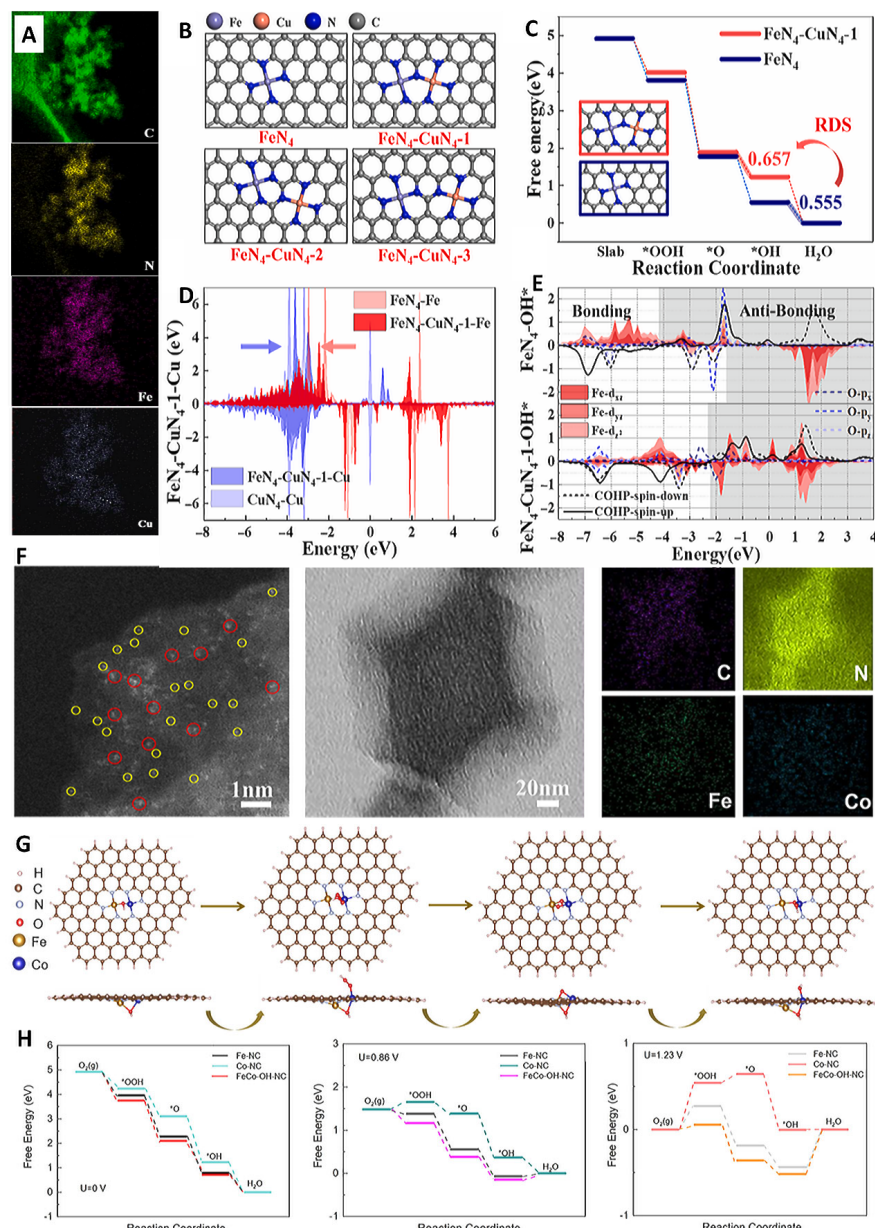


Figure 9. (A) Element mappings, (B) configurations diagram, and (C) free energy diagrams of FeN₄-CuN₄-1. (D) The d-band changes of Fe and Cu. (E) PDOS of the Fe and O orbitals [95]. Copyright © 2022, Elsevier Group. (F) AC-STEM image and elemental mapping; diatoms (red cycles), single atom (yellow cycles) (G) Side view and top view of the initial structures after adsorption. (H) Free energy for the ORR at a different potential [106]. Copyright © 2022, American Chemical Society.

3.3. Nanocluster Collaboration

Due to their adjustable electronic structure and excellent atomic utilization efficiency, SACs have attracted much attention [88]. However, there is still a need for continuous improvement in their single-atom activity and stability. Recent studies have shown that doping Fe-N-C materials with metal clusters can also improve their performance. In ORR catalysis research, metal nanoclusters can synergistically promote the activity of Fe-NC catalysts by adjusting their electronic structure and providing highly dispersed active sites, reducing the reaction energy barriers, improving the mass transfer performance of

Fe-NC catalysts, and increasing the diffusion efficiency of reactants, thereby significantly enhancing the activity and improving the stability. At the same time, nanoclusters (NCs) can stabilize the active sites of Fe-NC catalysts, provide a protective layer to reduce oxidation and corrosion of the catalyst during the reaction process, and prevent aggregation and deactivation under reaction conditions. For example, some NCs can promote the electronic transfer of Fe atoms, thereby enhancing their reduction ability. Commonly studied metal clusters include Fe [107–113], Cu [114–116], Pd [117–119], Co [120,121], Ni [122,123], etc.

Shui et al. reported a novel Fe-based electrocatalyst that simultaneously possesses N-coordinated Fe NCs and closely spaced Fe-N₄ active sites for acidic ORRs (Figure 10) [124]. In the thermal treatment process, N doping in carbonaceous support was used to achieve moderate coordination strength with metal elements while introducing Fe clusters, resulting in a uniform distribution of Fe monatomic and Fe NCs. The results show that there is a strong electron interaction between Fe NCs and Fe single atoms, and that Fe clusters can introduce OH ligands, reduce the ORR energy barrier and improve the performance of the Fe-N₄ site. In addition, the stability of Fe-N_x species at different temperatures was predicted. The study found that Fe clusters optimized the adsorption strength of oxygen-containing species on the Fe-N₄ site and shortened the amplitude of the Fe-N bonds of Fe-N₄ through non-coherent vibrations of Fe clusters and single atoms. Therefore, metal dissolution on Fe-N₄ sites was effectively suppressed, resulting in a 60% reduction in iron ion dissolution.

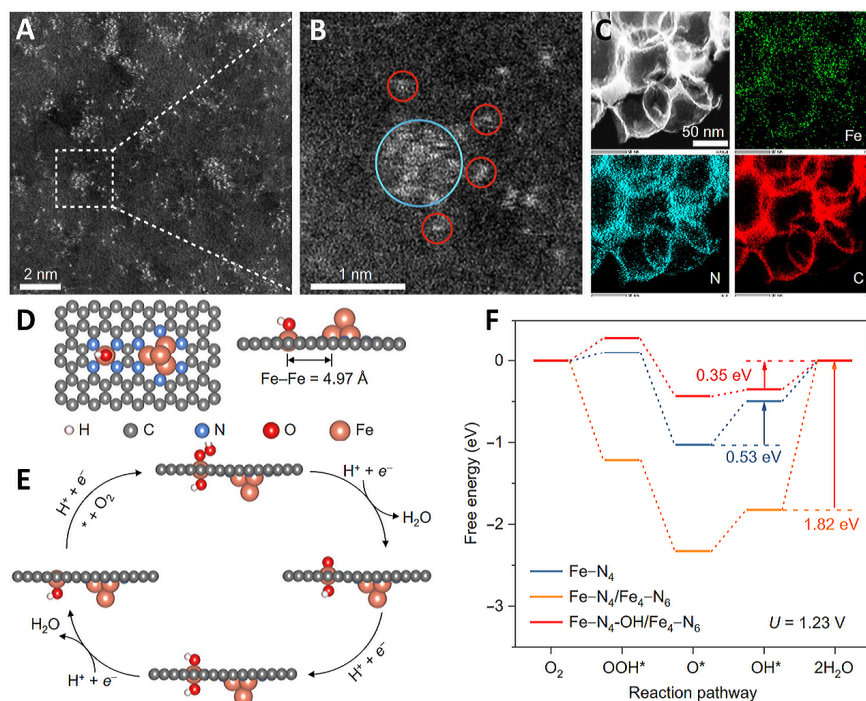


Figure 10. (A–C) HAADF-STEM image and corresponding element mappings; iron cluster (cyan circle) and iron atoms (red circles). (D) Model structure, (E) schematic ORR process. (F) Free energy diagrams of Fe-N₄, Fe-N₄/Fe₄-N₆, and Fe-N₄-OH/Fe₄-N₆ [124]. Copyright ©2022 Springer Nature.

Han et al. reported a novel catalyst with Fe-N₄ and Co₄ clusters on a nitrogen-doped carbon support by encapsulating the clusters in a carbonaceous MOF precursor (Figure 11) [125]. This catalyst regulated the electronic structure of Fe-N₄ through the Co₄ clusters, resulting in a high stability and ORR performance. DFT theoretical calculations showed that neighboring Co₄ clusters help to activate O₂ at the Fe-N₄ active site and reduce the adsorption of oxygen intermediates on Fe-N₄, thereby reducing the overpotential of Fe-N₄ during ORR and accelerating the overall ORR kinetics. Further charge density and d-band center theory results showed that the coupled Co₄ clusters significantly optimized

the electronic configuration of Fe-N₄ and controlled its adsorption of oxygen-containing species. Wei et al. reported on the preparation of a spin-state-tunable Fe single-atom catalyst (Figure 12) [126]. In terms of non-precious metal loading, the stability and activity of Fe/Pd-N-C are better than commercial Pt/C catalysts in acidic electrolytes, mainly due to the electronic structure differences between Pd NCs and Fe single atoms. This allows Pd NCs to successfully induce an electron transition from the d_{yz} orbital to the d_z² orbital in the Fe single atom, achieving the transition of Fe(II) from low to medium spin. Further theoretical calculations show that the medium spin is favorable to the side-pair adsorption mode of O₂, promoting the direct 4e⁻ pathway. At the same time, the occurrence of the 4e-dissociation pathway avoids the generation of H₂O₂, not only improving selectivity but also avoiding the attack of H₂O₂ on the active sites of Fe, carbon carriers, and proton exchange membranes, improving stability. In addition, the half-filled d_z² orbitals of the medium spin Fe(II) and the O 2p orbitals of OH^{*} generate σ* bonds that facilitate the rapid desorption of OH^{*}, effectively accelerating the entire ORR dynamics.

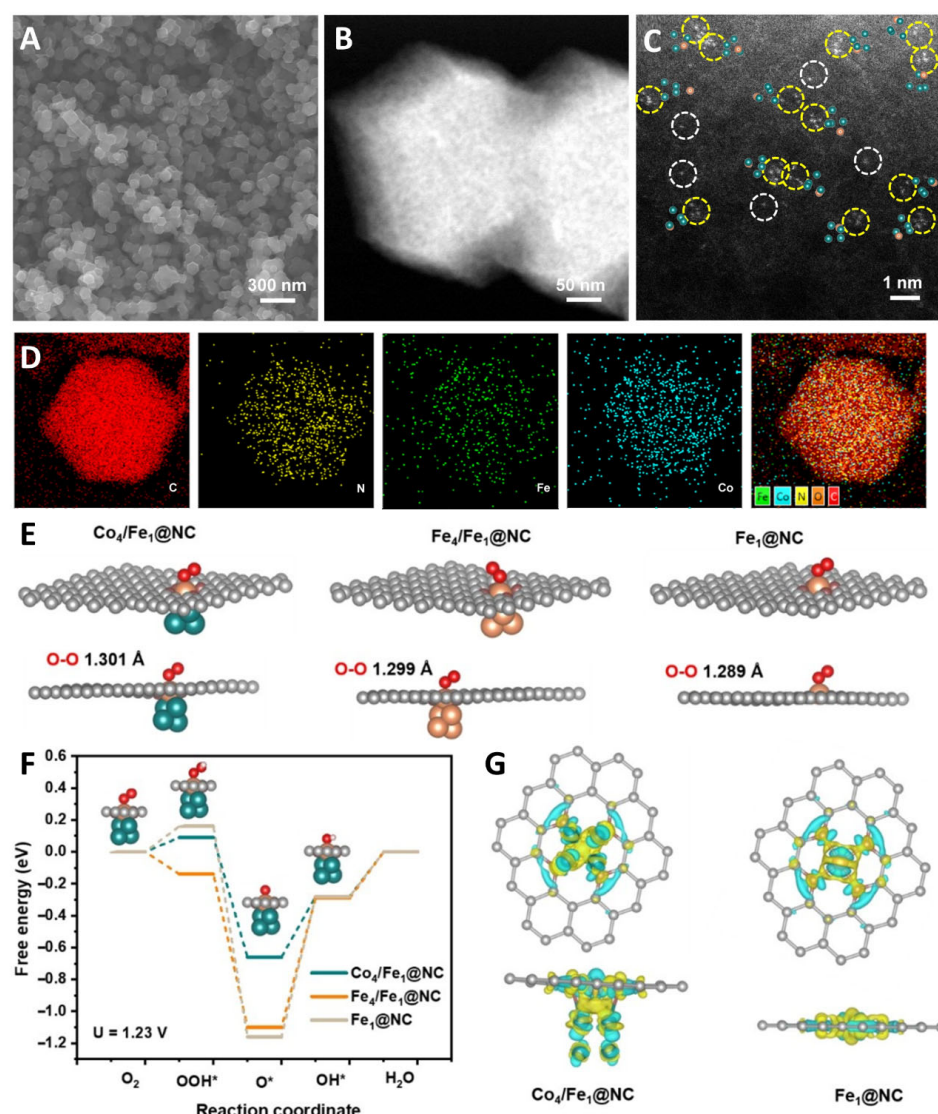


Figure 11. (A) SEM image, (B) aberration-corrected STEM image, (C) atomic-resolution HAADF-STEM image; C (red), N (yellow), Fe (green), Co (blue), (D) elemental mapping of Co₄/Fe₁@NC. Mechanism investigation of Co₄/Fe₁@NC. (E) O₂ adsorption models of Co₄/Fe₁@NC, Fe₄/Fe₁@NC and Fe₁@NC; (F) Gibbs free energy diagram for ORR on Co₄/Fe₁@NC, Fe₄/Fe₁@NC and Fe₁@NC, (G) Charge density of Co₄/Fe₁@NC and Fe₁@NC [125]. Copyright © 2023 Wiley & Sons.

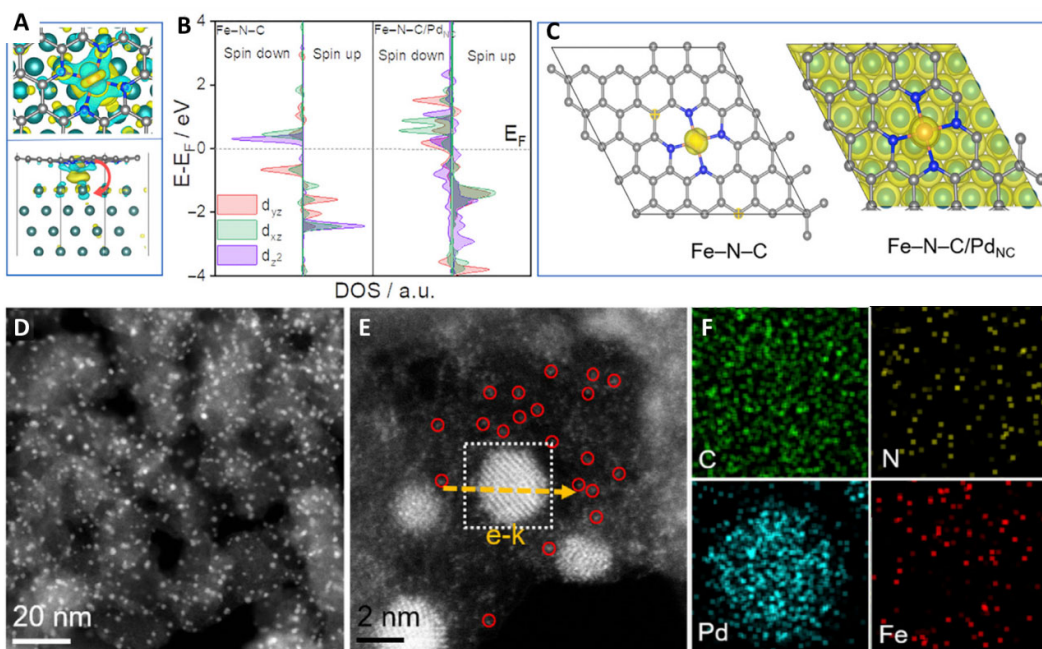


Figure 12. (A) Charge density difference, (B) DOS, (C) spin density of of Fe-N-C/Pd_{NC}. (D,E) HAADF-STEM image; Fe single atoms (red circles), Pd_{NC} (white box),mapping area (yellow arrows) (F) EDS elementary of Fe-N-C/Pd_{NC} [126]. Copyright ©2023 Cell Press.

3.4. Active Site Density Engineering

The activity of the catalyst is closely related to the properties of the catalyst material (such as nitrogen content and the dispersion of metal species) and the microstructure of the catalyst (such as porosity and packing structure). In general, the higher porosity of the catalyst means that more active sites can be exposed to ensure rapid electron transfer. High-nitrogen isomers also tend to provide more active sites, while increasing the density of highly dispersed metal monomers can also significantly improve the ORR activity. Therefore, the use of the active site is not only dependent on the type of catalyst material but is also strongly influenced by the final microstructure of the electrocatalysts and the density of the active site. Disordered stacked structures tend to restrict the mass transfer channels and reduce the exposure of the active sites. The abundant porous structure is conducive to full exposure of the active site and promotes easier proximity of gas molecules and oxygenated intermediates to the active site during the reaction [127].

To further improve the atomic utilization efficiency, Fe-N-C-based SACs can increase their ORR performance through active site density engineering [128,129], such as enhancing edge active sites [62,130], regulating structures [131–141], increasing loading [142,143], and other means to facilitate their performance. Yin et al. proposed a phosphorus-driven method to manipulate the electronic structure of edge FeN₄ active sites to enhance ORR performance. This report demonstrated for the first time that local electron redistribution makes a significant difference between edge-type FeN₄P₂ and in-plane FeN₄P₂ of different charge densities, and that defects in the FeN₄P₂ structure favor the selectivity of the four-electron ORR pathway (Figure 13) [62]. After the introduction of P atoms onto a carbon-based substrate, the charge density around FeN₄ undergoes a rearrangement and enhances the internal electronic conduction, thereby regulating the adsorption behavior of key intermediates. In particular, such delocalization can potentially cause atoms to be further apart, leading to significant interactions. The adjacent phosphorus active sites, which enhance activity, can drive significant long-range electronic delocalization of the Fe 3d center.

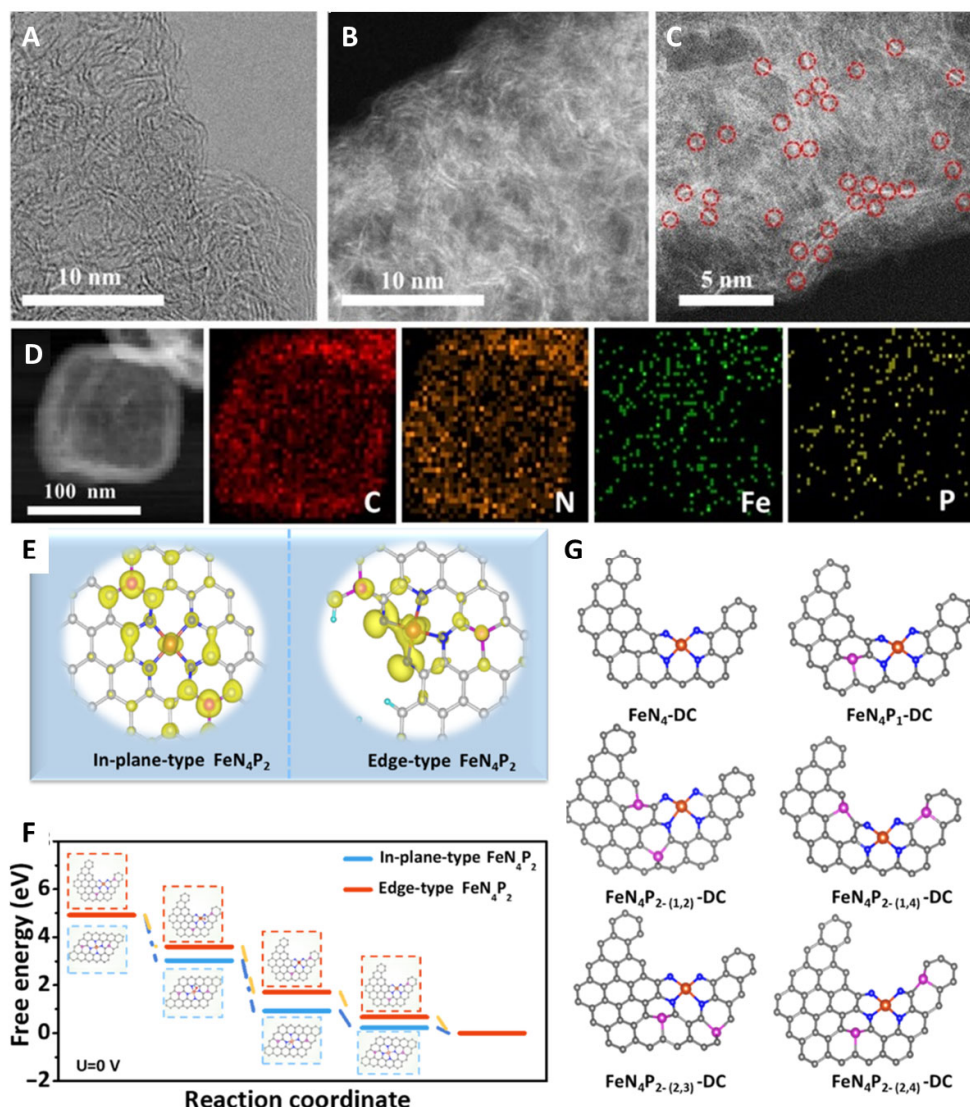


Figure 13. (A) HAADF-STEM images. (B–D) HRTEM image and the corresponding EDS elemental maps of Fe-N-C-P/N and P-C; circles (Fe-N-C-P SACs). (E) Differential charge densities, (F) free energy diagrams of in-plane-type and edge-type FeN₄P₂. (G) DFT models used for the stability calculations; Fe atoms (yellow), N atoms (blue), P atoms (carmine) [62]. Copyright © 2021 American Chemical Society.

Due to their unique electronic structure, SACs can effectively adsorb O₂ and catalyze the subsequent O-O bond cleavage. However, SACs still suffer from low metal loading, so increasing the metal loading on Fe-N-C-based catalysts can also improve their ORR performance. Jiang et al. reported a method for preparing catalysts with up to 9.8 wt.% metal loading of dense FeCo DACs on porous nitrogen-doped carbon nanofibers using plasma defect engineering (Figure 14A–F) [143]. This method generates a large number of defects in the N-doped carbon nanofiber, providing the opportunity for high metal loading. Benefiting from the synergistic effects of Fe Co dual metal atomic sites, the FeCo-N-C catalyst showed outstanding ORR performance. In addition, a series of characterizations have revealed the dynamic structure and valence state changes of the active sites. This report not only provides a new strategy for the fabrication of highly loaded Fe-N-C SACs but also provides a mechanism study of dual-metal SACs in ORRs.

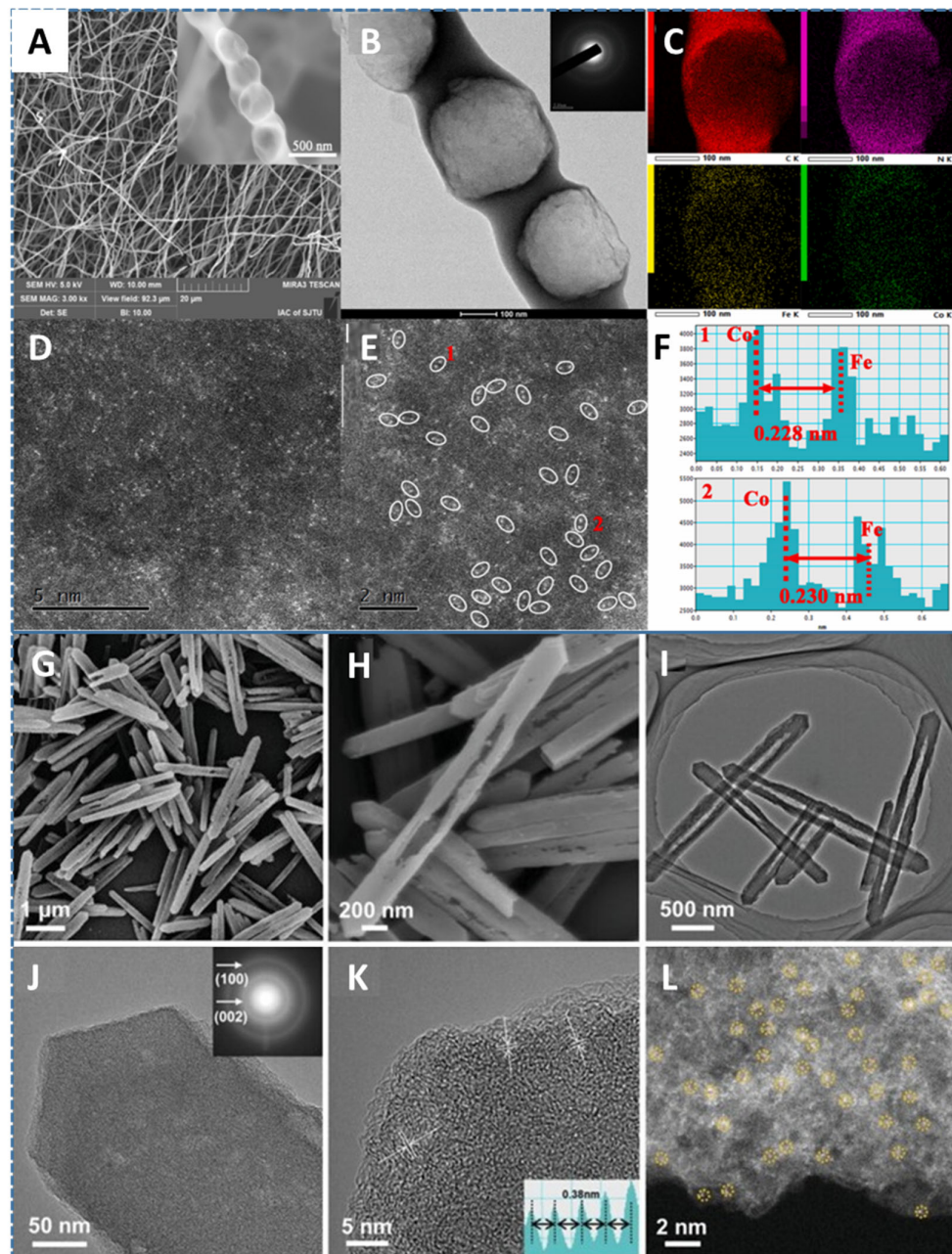


Figure 14. (A) SEM image, (B) TEM image, (C) EDS images, (D,E) HAADF-STEM images of Fe, Co SAs-PNCF, (F) distance of Fe, Co atom pair [143]. Copyright © 2022 Elsevier Inc. (G,H) SEM images, (I,J) TEM images, (K) HRTEM image, (L) HAADF-STEM image of Fe1-N-C HNRs; isolated Fe atoms (yellow dotted circles) [144]. Copyright © 2022, John Wiley & Sons.

Ma et al. synthesized an open-cavity ZIF-8 hollow nanostructure and transformed it into a nitrogen-doped carbon hollow nanostructure to load Fe-N₄ atomic active sites (Figure 14G–L) [144]. Compared with traditional ZIF-8-derived carbon, one-dimensional carbon nanomaterials have unique advantages due to their unique one-dimensional hollow structure, including efficient electronic transmission channels, a fast mass transfer, and a larger surface area. In addition, the high density of pyridine and graphite nitrogen doping can effectively regulate the microenvironment of the separated iron atoms, thereby reducing the activation energy barrier of the ORR process. These are effective methods for improving the ORR performance of Fe-N-C SACs. Notably, this catalyst also exhibits excellent performance in ZABs.

In addition, optimizing the degree of graphitization of carbon carriers is an effective strategy to potentially improve the oxidation resistance of carbon materials. The high degree of graphitization of the carbon carriers can further optimize the performance of the carbon materials. Highly graphitized carbon materials have a higher electrical conductivity, which helps to promote electron transfer in the reaction and can meet the requirements of various applications. Secondly, increasing the degree of graphitization of carbon materials can help to improve the oxidation resistance of catalysts, which can prolong their lifetime and reduce the performance degradation caused by oxidation [145–147]. Kang et al. reported an effective strategy (pyrolysis in high-temperature conditions (1100–1200 °C)) to significantly improve the stability of Fe-N-C catalysts. Pyrolysis in this temperature range allowed for the removal of the low-activity nitrogen atom uncoordinated sites, which are prone to produce harmful H₂O₂ side reaction products, and at the same time, it was possible to convert the less stable D1 site (O-FeN₄C₁₂) to the more stable D2 structural site (FeN₄C₁₀) in this temperature range [148]. Table 1 summarizes the performance of some recent atomically dispersed Fe-based ORR catalysts in different electrolytic media.

Table 1. Comparison of the ORR performance of reported Fe-based catalysts.

Catalysts	Electrolyte	Half-Wave (V vs. RHE)	Current Intensity mA cm ⁻²	Reference
Fe ₂ -NC	0.1 M HClO ₄	0.78	5.5	[149]
Fe _{SA} /Fe _{AC} -NC 900	0.1 M HClO ₄	0.80	5.5	[107]
FeNi-N6	0.1 M HClO ₄	0.79	5.2	[150]
M/FeCo-SAs-N-C	0.1 M HClO ₄	0.851	4.7	[151]
Co ₂ /Fe-N@CHC	0.1 M HClO ₄	0.812	5.9	[152]
FeN ₄ Cl SAC	0.1 M HClO ₄	0.818	6.0	[153]
Fe-N/S-C-10%	0.5 M H ₂ SO ₄	0.81	4.9	[154]
Fe-N-S CNN	0.5 M H ₂ SO ₄	0.78	6.0	[155]
Fe _{NCs} /Fe _{SAs} -NC-Z8@34	0.1 M KOH	0.918	5.6	[108]
FeS/FeNSC	0.1 M KOH	0.91	5.3	[156]
Fe _P -DAS@MPC	0.1 M KOH	0.92	6.5	[66]
Fe@Fe/N-G-80	0.1 M KOH	0.866	6.34	[157]
Fe _{ACs} /NPS HC	0.1 M KOH	0.87	6.0	[158]

4. Conclusions and Outlook

Efficient and stable electrocatalysts play a crucial role in energy conversion. This article reviews the active sources and degradation mechanisms of atomic Fe-N-C SACs, as well as common modification strategies. Although significant progress has been made in ORR performance, the stability of M-N-C electrocatalysts still lags behind that of Pt/C. It is worth noting that the aim of M-N-C ORR electrocatalyst research should be to improve the catalyst to reduce the mass transfer loss under a high current density, and to further develop efficient hybrid/composite catalysts to improve their activity and durability in order to achieve successful application in PEMFCs. The key to replacing PGM catalysts with Fe-N-C catalysts lies in their atomic dispersion, abundant active centers, and high mass transport efficiency.

Future research must also focus on the following points:

- (1) The precise design of the doping sites and the uniform distribution of the separated metal atoms require further research. There is an urgent need to increase the loading of individual metal atoms so that more individual atoms can be anchored to the substrate, resulting in greater activity and durability.
- (2) Further research on different substrates is needed for the selection of an ideal, low-cost, stable support to improve the active site exposure and environmental stability of the catalyst. High-surface-area and high-volume porous carbon substrates are excellent substrates for active sites. A good substrate should be able to precisely regulate the physical/chemical environment to provide stronger bonds for isolated iron atoms,

- thereby maintaining stronger catalytic activity in the electrocatalytic process and ensuring long-term performance during the electrocatalytic process.
- (3) In the design and preparation of catalysts, the framework structure and interatomic interactions of the support should be fully considered in order to maximize the dispersion of metal atoms, effectively suppress the aggregation of metal atoms, and reduce the loss of active sites. The scope of research on dopants should be further extended, and the effects of these impurities at different doping sites should be fully and accurately considered.
- (4) Theoretical calculations and *in situ* characterization techniques should be used to further explore the relationship between structure and performance at the atomic level and to promote research into catalytic mechanisms. Advanced systematic testing methods are key factors in the rational evaluation of catalyst performance. With precise control of the coordination environment, Fe-N-C catalysts have broad application prospects in areas such as fuel cells (FCs).

In conclusion, the development of novel modified Fe-N-C catalysts for ORR is crucial, but in-depth research on catalyst synthesis, active sites, and reaction pathways is needed. In addition, theoretical simulations and experimental research should be systematically combined to elucidate the core control principles and reaction mechanisms of Fe-N-C catalysts and to reveal the changes in catalytic selectivity during catalyst design and optimization. The in-depth exploration of the relationship between the structure of Fe-N-C SACs and catalytic theory will provide insights into the design and optimization of energy conversion catalysts and help us to achieve green energy storage and conversion.

Author Contributions: Conceptualization, Y.L. (Yao Lin) and J.B.; investigation, J.X., Y.L. (Yao Lin) and W.Z.; resources, Y.L. (Yuebin Lian) and J.B.; writing—original draft preparation, Y.L. (Yuebin Lian); writing—review and editing, Y.L. (Yuebin Lian) and J.B.; supervision, J.B.; funding acquisition, Y.L. (Yuebin Lian). All authors have read and agreed to the published version of the manuscript.

Funding: This research was funded by the National Natural Science Foundation of China (No. 22202020), Natural Science Research Project of Jiangsu Higher Education Institutions of China (No. 21KJB430018), and China Postdoctoral Science Foundation (No. 2022M722307).

Institutional Review Board Statement: Not applicable.

Informed Consent Statement: Not applicable.

Data Availability Statement: Not applicable.

Conflicts of Interest: The authors declare no conflicts of interest.

References

- Snitkoff-Sol, R.Z.; Friedman, A.; Honig, H.C.; Yurko, Y.; Kozhushner, A.; Zachman, M.J.; Zelenay, P.; Bond, A.M.; Elbaz, L. Quantifying the electrochemical active site density of precious metal-free catalysts *in situ* in fuel cells. *Nat. Catal.* **2022**, *5*, 163–170. [[CrossRef](#)]
- Sun, W.; Wang, F.; Zhang, B.; Zhang, M.; Kupers, V.; Ji, X.; Theile, C.; Bieker, P.; Xu, K.; Wang, C.; et al. A rechargeable zinc-air battery based on zinc peroxide chemistry. *Science* **2021**, *371*, 46–51. [[CrossRef](#)] [[PubMed](#)]
- Mehmood, A.; Gong, M.; Jaouen, F.; Roy, A.; Zitolo, A.; Khan, A.; Sougrati, M.-T.; Primbs, M.; Bonastre, A.M.; Fongalland, D.; et al. High loading of single atomic iron sites in Fe–NC oxygen reduction catalysts for proton exchange membrane fuel cells. *Nat. Catal.* **2022**, *5*, 311–323. [[CrossRef](#)]
- Zhu, Y.; Yue, K.; Xia, C.; Zaman, S.; Yang, H.; Wang, X.; Yan, Y.; Xia, B.Y. Recent Advances on MOF Derivatives for Non-Noble Metal Oxygen Electrocatalysts in Zinc-Air Batteries. *Nano-Micro Lett.* **2021**, *13*, 137. [[CrossRef](#)] [[PubMed](#)]
- Li, L.; Li, N.; Xia, J.-W.; Zhou, S.-L.; Qian, X.-Y.; Yin, F.-X.; Dai, G.-H.; He, G.-Y.; Chen, H.-Q. A pH-universal ORR catalyst with atomic Fe-heteroatom (N, S) sites for high-performance Zn-air batteries. *Nano Res.* **2023**, *16*, 9416–9425. [[CrossRef](#)]
- Wang, Y.; Hao, J.; Liu, Y.; Liu, M.; Sheng, K.; Wang, Y.; Yang, J.; Li, J.; Li, W. Recent advances in regulating the performance of acid oxygen reduction reaction on carbon-supported non-precious metal single atom catalysts. *J. Energy Chem.* **2023**, *76*, 601–616. [[CrossRef](#)]
- Ren, S.; Duan, X.; Ge, F.; Chen, Z.; Yang, Q.; Zhang, M.; Zheng, H. Novel MOF-derived hollow CoFe alloy coupled with N-doped Ketjen Black as boosted bifunctional oxygen catalysts for Zn-air batteries. *Chem. Eng. J.* **2022**, *427*, 131614. [[CrossRef](#)]

8. Yang, Z.; Xiang, M.; Zhu, Y.; Hui, J.; Jiang, Y.; Dong, S.; Yu, C.; Ou, J.; Qin, H. Single-atom platinum or ruthenium on C₄N as 2D high-performance electrocatalysts for oxygen reduction reaction. *Chem. Eng. J.* **2021**, *426*, 131347. [[CrossRef](#)]
9. Pruchyathamkorn, J.; Yang, M.; Amin, H.M.A.; Batchelor-McAuley, C.; Compton, R.G. Imaging Electrode Heterogeneity Using Chemically Confined Fluorescence Electrochemical Microscopy. *J. Phys. Chem. Lett.* **2017**, *8*, 6124–6127. [[CrossRef](#)]
10. Zhang, N.; Zhou, T.; Ge, J.; Lin, Y.; Du, Z.; Zhong, C.; Wang, W.; Jiao, Q.; Yuan, R.; Tian, Y.; et al. High-Density Planar-like Fe₂N₆ Structure Catalyzes Efficient Oxygen Reduction. *Matter* **2020**, *3*, 509–521. [[CrossRef](#)]
11. Zhang, Y.; Zhang, X.; Li, Y.; Wang, J.; Kawi, S.; Zhong, Q. FeCo alloy/N, S co-doped carbon aerogel derived from directional-casting cellulose nanofibers for rechargeable liquid flow and flexible Zn-air batteries. *Nano Res.* **2023**, *16*, 6870–6880. [[CrossRef](#)]
12. Yang, B.; Li, B.; Xiang, Z. Advanced MOF-based electrode materials for supercapacitors and electrocatalytic oxygen reduction. *Nano Res.* **2022**, *16*, 1338–1361. [[CrossRef](#)]
13. Sarapuu, A.; Lilloja, J.; Akula, S.; Zagal, J.H.; Specchia, S.; Tammeveski, K. Recent Advances in Non-Precious Metal Single-Atom Electrocatalysts for Oxygen Reduction Reaction in Low-Temperature Polymer-Electrolyte Fuel Cells. *ChemCatChem* **2023**, *15*, e202300849. [[CrossRef](#)]
14. Bai, J.; Ge, W.; Zhou, P.; Xu, P.; Wang, L.; Zhang, J.; Jiang, X.; Li, X.; Zhou, Q.; Deng, Y. Precise constructed atomically dispersed Fe/Ni sites on porous nitrogen-doped carbon for oxygen reduction. *J. Colloid Interface Sci.* **2022**, *616*, 433–439. [[CrossRef](#)] [[PubMed](#)]
15. Ku, Y.P.; Ehelebe, K.; Hutzler, A.; Bierling, M.; Bohm, T.; Zitolo, A.; Vorokhta, M.; Bibent, N.; Speck, F.D.; Seeberger, D.; et al. Oxygen Reduction Reaction in Alkaline Media Causes Iron Leaching from Fe-N-C Electrocatalysts. *J. Am. Chem. Soc.* **2022**, *144*, 9753–9763. [[CrossRef](#)] [[PubMed](#)]
16. Xie, X.; He, C.; Li, B.; He, Y.; Cullen, D.A.; Wegener, E.C.; Kropf, A.J.; Martinez, U.; Cheng, Y.; Engelhard, M.H.; et al. Performance enhancement and degradation mechanism identification of a single-atom Co-N-C catalyst for proton exchange membrane fuel cells. *Nat. Catal.* **2020**, *3*, 1044–1054. [[CrossRef](#)]
17. Zhan, Y.; Zeng, H.; Zhao, T.; Situ, A.; Yang, L.; Zhang, Z. Densely accessible single atom Fe sites dispersed on porous carbon as highly stable and active ORR catalyst for PEMFC. *Int. J. Hydrogen Energy* **2024**, *56*, 1049–1056. [[CrossRef](#)]
18. Tian, H.; Song, A.; Zhang, P.; Sun, K.; Wang, J.; Sun, B.; Fan, Q.; Shao, G.; Chen, C.; Liu, H.; et al. High Durability of Fe-N-C Single Atom Catalysts with Carbon Vacancies Towards Oxygen Reduction Reaction in Alkaline Media. *Adv. Mater.* **2023**, *35*, e2210714. [[CrossRef](#)]
19. Liu, H.; Jiang, L.; Khan, J.; Wang, X.; Xiao, J.; Zhang, H.; Xie, H.; Li, L.; Wang, S.; Han, L. Decorating Single-Atomic Mn Sites with FeMn Clusters to Boost Oxygen Reduction Reaction. *Angew. Chem. Int. Ed.* **2023**, *62*, e202214988. [[CrossRef](#)]
20. Zhuang, Z.; Xia, L.; Huang, J.; Zhu, P.; Li, Y.; Ye, C.; Xia, M.; Yu, R.; Lang, Z.; Zhu, J.; et al. Continuous Modulation of Electrocatalytic Oxygen Reduction Activities of Single-Atom Catalysts through p-n Junction Rectification. *Angew. Chem. Int. Ed.* **2023**, *62*, e202212335. [[CrossRef](#)]
21. Yang, H.; Liu, Y.; Liu, X.; Wang, X.; Tian, H.; Waterhouse, G.I.N.; Kruger, P.E.; Telfer, S.G.; Ma, S. Large-scale synthesis of N-doped carbon capsules supporting atomically dispersed iron for efficient oxygen reduction reaction electrocatalysis. *eScience* **2022**, *2*, 227–234. [[CrossRef](#)]
22. Chen, C.; Wu, Y.; Li, X.; Ye, Y.; Li, Z.; Zhou, Y. Modulating Fe spin state in FeNC catalysts by adjacent Fe atomic clusters to facilitate oxygen reduction reaction in proton exchange membrane fuel cell. *Appl. Catal. B-Environ.* **2024**, *342*, 123407. [[CrossRef](#)]
23. Xia, D.; Tang, X.; Dai, S.; Ge, R.; Rykov, A.; Wang, J.; Huang, T.H.; Wang, K.W.; Wei, Y.; Zhang, K.; et al. Ultrastable Fe-N-C Fuel Cell Electrocatalysts by Eliminating Non-Coordinating Nitrogen and Regulating Coordination Structures at High Temperatures. *Adv. Mater.* **2022**, *35*, e2204474. [[CrossRef](#)] [[PubMed](#)]
24. Zhu, R.; Qin, Y.; Wu, T.; Ding, S.; Su, Y. Insights into local coordination environment of main group metal-nitrogen-carbon catalysts for enhanced oxygen reduction reaction. *Appl. Surf. Sci.* **2023**, *631*, 157581. [[CrossRef](#)]
25. Qin, Y.; Li, Y.; Zhao, W.; Chen, S.; Wu, T.; Su, Y. Computational study of transition metal single-atom catalysts supported on nitrogenated carbon nanotubes for electrocatalytic nitrogen reduction. *Nano Res.* **2022**, *16*, 325–333. [[CrossRef](#)]
26. Ramaswamy, N.; Tylus, U.; Jia, Q.; Mukerjee, S. Activity descriptor identification for oxygen reduction on nonprecious electrocatalysts: Linking surface science to coordination chemistry. *J. Am. Chem. Soc.* **2013**, *135*, 15443–15449. [[CrossRef](#)] [[PubMed](#)]
27. Luo, G.; Wang, Y.; Li, Y. Two-dimensional iron-porphyrin sheet as a promising catalyst for oxygen reduction reaction: A computational study. *Sci. Bull.* **2017**, *62*, 1337–1343. [[CrossRef](#)] [[PubMed](#)]
28. Xu, H.; Cheng, D.; Cao, D.; Zeng, X.C. A universal principle for a rational design of single-atom electrocatalysts. *Nat. Catal.* **2018**, *1*, 339–348. [[CrossRef](#)]
29. Liu, K.; Fu, J.; Lin, Y.; Luo, T.; Ni, G.; Li, H.; Lin, Z.; Liu, M. Insights into the activity of single-atom Fe-N-C catalysts for oxygen reduction reaction. *Nat. Commun.* **2022**, *13*, 2075. [[CrossRef](#)]
30. Li, J.; Zhang, H.; Samarakoon, W.; Shan, W.; Cullen, D.A.; Karakalos, S.; Chen, M.; Gu, D.; More, K.L.; Wang, G.; et al. Thermally Driven Structure and Performance Evolution of Atomically Dispersed FeN₄ Sites for Oxygen Reduction. *Angew. Chem. Int. Ed.* **2019**, *58*, 18971–18980. [[CrossRef](#)]
31. Li, J.; Jiao, L.; Wegener, E.; Richard, L.L.; Liu, E.; Zitolo, A.; Sougrati, M.T.; Mukerjee, S.; Zhao, Z.; Huang, Y.; et al. Evolution Pathway from Iron Compounds to Fe₁(II)-N₄ Sites through Gas-Phase Iron during Pyrolysis. *J. Am. Chem. Soc.* **2020**, *142*, 1417–1423. [[CrossRef](#)] [[PubMed](#)]

32. Hu, X.; Chen, S.; Chen, L.; Tian, Y.; Yao, S.; Lu, Z.; Zhang, X.; Zhou, Z. What is the Real Origin of the Activity of Fe-N-C Electrocatalysts in the O₂ Reduction Reaction? Critical Roles of Coordinating Pyrrolic N and Axially Adsorbing Species. *J. Am. Chem. Soc.* **2022**, *144*, 18144–18152. [CrossRef] [PubMed]
33. Liu, S.; Li, C.; Zachman, M.J.; Zeng, Y.; Yu, H.; Li, B.; Wang, M.; Braaten, J.; Liu, J.; Meyer, H.M.; et al. Atomically dispersed iron sites with a nitrogen–carbon coating as highly active and durable oxygen reduction catalysts for fuel cells. *Nat. Energy* **2022**, *7*, 652–663. [CrossRef]
34. Meyer, Q.; Liu, S.; Li, Y.; Zhao, C. Operando detection of oxygen reduction reaction kinetics of Fe-N-C catalysts in proton exchange membrane fuel cells. *J. Power Sources* **2022**, *533*, 231058. [CrossRef]
35. Ma, Q.; Jin, H.; Zhu, J.; Li, Z.; Xu, H.; Liu, B.; Zhang, Z.; Ma, J.; Mu, S. Stabilizing Fe-N-C Catalysts as Model for Oxygen Reduction Reaction. *Adv. Sci.* **2021**, *8*, e2102209. [CrossRef]
36. Liu, S.; Meyer, Q.; Jia, C.; Wang, S.; Rong, C.; Nie, Y.; Zhao, C. Operando deconvolution of the degradation mechanisms of iron–nitrogen–carbon catalysts in proton exchange membrane fuel cells. *Energy Environ. Sci.* **2023**, *16*, 3792–3802. [CrossRef]
37. Li, J.K.; Sougrati, M.T.; Zitolo, A.; Ablett, J.M.; Oguz, I.C.; Mineva, T.; Matanovic, I.; Atanassov, P.; Huang, Y.; Zenyuk, I.; et al. Identification of durable and non-durable FeNx sites in Fe-N-C materials for proton exchange membrane fuel cells. *Nat. Catal.* **2020**, *4*, 10–19. [CrossRef]
38. Bae, G.; Kim, M.M.; Han, M.H.; Cho, J.; Kim, D.H.; Sougrati, M.-T.; Kim, J.; Lee, K.-S.; Joo, S.H.; Goddard, W.A.; et al. Unravelling the complex causality behind Fe-N-C degradation in fuel cells. *Nat. Catal.* **2023**, *6*, 1140–1150. [CrossRef]
39. Yarlagadda, V.; Carpenter, M.K.; Moylan, T.E.; Kukreja, R.S.; Koestner, R.; Gu, W. Boosting Fuel Cell Performance with Accessible Carbon Mesopores. *ACS Energy Lett.* **2018**, *3*, 618–621. [CrossRef]
40. Cheng, Y.; He, S.; Veder, J.P.; De Marco, R.; Yang, S.Z.; Jiang, S.P. Atomically Dispersed Bimetallic FeNi Catalysts as Highly Efficient Bifunctional Catalysts for Reversible Oxygen Evolution and Oxygen Reduction Reactions. *ChemElectroChem* **2019**, *6*, 3478–3487. [CrossRef]
41. Cao, Y.; Zhang, Y.; Yang, L.; Zhu, K.; Yuan, Y.; Li, G.; Yuan, Y.; Zhang, Q.; Bai, Z. Boosting oxygen reduction reaction kinetics through perturbing electronic structure of single-atom Fe-N₃S₁ catalyst with sub-nano FeS cluster. *J. Colloid Interface Sci.* **2023**, *650*, 924–933. [CrossRef] [PubMed]
42. Cui, L.; Hao, J.; Zhang, Y.; Kang, X.; Zhang, J.; Fu, X.Z.; Luo, J.L. N and S dual-coordinated Fe single-atoms in hierarchically porous hollow nanocarbon for efficient oxygen reduction. *J. Colloid Interface Sci.* **2023**, *650*, 603–612. [CrossRef] [PubMed]
43. Li, G.; Tang, Y.; Fu, T.; Xiang, Y.; Xiong, Z.; Si, Y.; Guo, C.; Jiang, Z. S, N co-doped carbon nanotubes coupled with CoFe nanoparticles as an efficient bifunctional ORR/OER electrocatalyst for rechargeable Zn-air batteries. *Chem. Eng. J.* **2022**, *429*, 132174. [CrossRef]
44. Li, Z.; Zhang, L.; Zhu, Q.; Ke, Z.; Hu, G. Spatial separation strategy to construct N/S co-doped carbon nanobox embedded with asymmetrically coupled Fe-Co pair-site for boosted reversible oxygen electrocatalysis. *J. Energy Chem.* **2024**, *653*, 1577–1587. [CrossRef] [PubMed]
45. Fu, X.; Zhang, L.; Zhu, X.; Zhu, S.; Min, Y.; Xu, Q.; Li, Q. Trace Mn-doped on highly dispersed Fe/Mn-SNC ultrathin carbon nanosheets for efficient oxygen reduction reaction. *Appl. Surf. Sci.* **2023**, *613*, 156087. [CrossRef]
46. Wang, R.; Liu, J.; Xie, J.; Cai, Z.; Yu, Y.; Zhang, Z.; Meng, X.; Wang, C.; Xu, X.; Zou, J. Hollow nanocage with skeleton Ni-Fe sulfides modified by N-doped carbon quantum dots for enhancing mass transfer for oxygen electrocatalysis in zinc-air battery. *Appl. Catal. B-Environ.* **2023**, *324*, 122230. [CrossRef]
47. Mun, Y.; Lee, S.; Kim, K.; Kim, S.; Lee, S.; Han, J.W.; Lee, J. Versatile Strategy for Tuning ORR Activity of a Single Fe-N₄ Site by Controlling Electron-Withdrawing/Donating Properties of a Carbon Plane. *J. Am. Chem. Soc.* **2019**, *141*, 6254–6262. [CrossRef] [PubMed]
48. Bai, X.; Wang, Y.; Han, J.; Niu, X.; Guan, J. Engineering the electronic structure of isolated manganese sites to improve the oxygen reduction, Zn-air battery and fuel cell performances. *Appl. Catal. B-Environ.* **2023**, *337*, 122966. [CrossRef]
49. Xiao, Z.; Wu, Y.; Cao, S.; Yan, W.; Chen, B.; Xing, T.; Li, Z.; Lu, X.; Chen, Y.; Wang, K.; et al. An active site pre-anchoring and post-exposure strategy in Fe(CN)₆⁴⁻@PPy derived Fe/S/N-doped carbon electrocatalyst for high performance oxygen reduction reaction and zinc-air batteries. *Chem. Eng. J.* **2021**, *413*, 127395. [CrossRef]
50. Yang, Y.; Xu, X.; Sun, P.; Xu, H.; Yang, L.; Zeng, X.; Huang, Y.; Wang, S.; Cao, D. AgNPs@Fe-N-C oxygen reduction catalysts for anion exchange membrane fuel cells. *Nano Energy* **2022**, *100*, 107466. [CrossRef]
51. Li, Y.; Zang, K.; Duan, X.; Luo, J.; Chen, D. Boost oxygen reduction reaction performance by tuning the active sites in Fe-N-P-C catalysts. *J. Energy Chem.* **2021**, *55*, 572–579. [CrossRef]
52. Ma, R.; Cui, X.; Xu, X.; Wang, Y.; Xiang, G.; Gao, L.; Lin, Z.; Yang, Y. Collaborative integration of ultrafine Fe₂P nanocrystals into Fe, N, P-codoped carbon nanoshells for highly-efficient oxygen reduction. *Nano Energy* **2023**, *108*, 108179. [CrossRef]
53. An, Q.; Zhang, X.; Yang, C.; Su, H.; Zhou, W.; Liu, M.; Zhang, X.; Sun, X.; Bo, S.; Yu, F.; et al. Engineering Unsymmetrically Coordinated Fe Sites via Heteroatom Pairs Synergetic Contribution for Efficient Oxygen Reduction. *Small* **2023**, *19*, e2304303. [CrossRef] [PubMed]
54. Chang, H.; Guo, Y.-F.; Liu, X.; Wang, P.-F.; Xie, Y.; Yi, T.-F. Dual MOF-derived Fe/N/P-tridoped carbon nanotube as high-performance oxygen reduction catalysts for zinc-air batteries. *Appl. Catal. B-Environ.* **2023**, *327*, 122469. [CrossRef]
55. Xu, L.-H.; Che, P.-C.; Zhang, X.-J.; Cosnier, S.; Shan, D. FeP nanoparticles highly dispersed on N,P-doped petaloid carbon nanosheet: Interface engineering and boosted intrinsic ORR activity. *Appl. Surf. Sci.* **2023**, *620*, 156770. [CrossRef]

56. Liu, H.; Jiang, L.; Sun, Y.; Khan, J.; Feng, B.; Xiao, J.; Zhang, H.; Xie, H.; Li, L.; Wang, S.; et al. Asymmetric N, P-Coordinated Single-Atomic Fe Sites with Fe_2P Nanoclusters/Nanoparticles on Porous Carbon Nanosheets for Highly Efficient Oxygen Electroreduction. *Adv. Energy Mater.* **2023**, *13*, 2301223. [[CrossRef](#)]
57. Pei, Z.; Zhang, H.; Guo, Y.; Luan, D.; Gu, X.; Lou, X.W.D. Atomically Dispersed Fe Sites Regulated by Adjacent Single Co Atoms Anchored on N-P Co-Doped Carbon Structures for Highly Efficient Oxygen Reduction Reaction. *Adv. Mater.* **2023**, *e2306047*. [[CrossRef](#)] [[PubMed](#)]
58. Xue, W.; Zhou, Q.; Cui, X.; Zhang, J.; Zuo, S.; Mo, F.; Jiang, J.; Zhu, X.; Lin, Z. Atomically Dispersed FeN_2P_2 Motif with High Activity and Stability for Oxygen Reduction Reaction Over the Entire pH Range. *Angew. Chem. Int. Ed.* **2023**, *62*, e202307504. [[CrossRef](#)]
59. Zhang, Q.; Tsai, H.J.; Li, F.; Wei, Z.; He, Q.; Ding, J.; Liu, Y.; Lin, Z.Y.; Yang, X.; Chen, Z.; et al. Boosting the Proton-coupled Electron Transfer via Fe-P Atomic Pair for Enhanced Electrochemical CO_2 Reduction. *Angew. Chem. Int. Ed.* **2023**, *135*, e202311550. [[CrossRef](#)]
60. Zhou, Y.; Lu, R.; Tao, X.; Qiu, Z.; Chen, G.; Yang, J.; Zhao, Y.; Feng, X.; Mullen, K. Boosting Oxygen Electrocatalytic Activity of Fe-N-C Catalysts by Phosphorus Incorporation. *J. Am. Chem. Soc.* **2023**, *145*, 3647–3655. [[CrossRef](#)]
61. Roh, J.; Cho, A.; Kim, S.; Lee, K.-S.; Shin, J.; Choi, J.S.; Bak, J.; Lee, S.; Song, D.; Kim, E.-J.; et al. Transformation of the Active Moiety in Phosphorus-Doped Fe-N-C for Highly Efficient Oxygen Reduction Reaction. *ACS Catal.* **2023**, *13*, 9427–9441. [[CrossRef](#)]
62. Yin, H.; Yuan, P.; Lu, B.-A.; Xia, H.; Guo, K.; Yang, G.; Qu, G.; Xue, D.; Hu, Y.; Cheng, J.; et al. Phosphorus-Driven Electron Delocalization on Edge-Type FeN_4 Active Sites for Oxygen Reduction in Acid Medium. *ACS Catal.* **2021**, *11*, 12754–12762. [[CrossRef](#)]
63. Xu, J.; Zhang, S.; Liu, H.; Liu, S.; Yuan, Y.; Meng, Y.; Wang, M.; Shen, C.; Peng, Q.; Chen, J.; et al. Breaking Local Charge Symmetry of Iron Single Atoms for Efficient Electrocatalytic Nitrate Reduction to Ammonia. *Angew. Chem. Int. Ed.* **2023**, *62*, e202308044. [[CrossRef](#)] [[PubMed](#)]
64. Sun, X.; Tuo, Y.; Ye, C.; Chen, C.; Lu, Q.; Li, G.; Jiang, P.; Chen, S.; Zhu, P.; Ma, M.; et al. Phosphorus Induced Electron Localization of Single Iron Sites for Boosted CO_2 Electroreduction Reaction. *Angew. Chem. Int. Ed.* **2021**, *60*, 23614–23618. [[CrossRef](#)] [[PubMed](#)]
65. He, Y.; Jia, Y.; Yu, B.; Wang, Y.; Li, H.; Liu, Y.; Tan, Q. Heteroatom Coordination Regulates Iron Single-Atom-Catalyst with Superior Oxygen Reduction Reaction Performance for Aqueous Zn-Air Battery. *Small* **2023**, *19*, e2206478. [[CrossRef](#)] [[PubMed](#)]
66. Zong, L.; Fan, K.; Li, P.; Lu, F.; Li, B.; Wang, L. Promoting Oxygen Reduction Reaction on Atomically Dispersed Fe Sites via Establishing Hydrogen Bonding with the Neighboring P Atoms. *Adv. Energy Mater.* **2023**, *13*, 2203611. [[CrossRef](#)]
67. Zhang, J.; Huang, Q.-a.; Wang, J.; Wang, J.; Zhang, J.; Zhao, Y. Supported dual-atom catalysts: Preparation, characterization, and potential applications. *Chin. J. Catal.* **2020**, *41*, 783–798. [[CrossRef](#)]
68. Zeng, Z.; Gan, L.Y.; Yang, H.B.; Su, X.; Gao, J.; Liu, W. Orbital coupling of hetero-diatom nickel-iron site for bifunctional electrocatalysis of CO_2 reduction and oxygen evolution. *Nat. Commun.* **2021**, *12*, 4088. [[CrossRef](#)]
69. Hao, Q.; Zhong, H.-X.; Wang, J.-Z.; Liu, K.-H.; Yan, J.-M.; Ren, Z.-H. Nickel dual-atom sites for electrochemical carbon dioxide reduction. *Nat. Synth.* **2022**, *1*, 719–728. [[CrossRef](#)]
70. Tang, T.; Wang, Y.; Han, J.; Zhang, Q.; Bai, X.; Niu, X. Dual-atom Co-Fe catalysts for oxygen reduction reaction. *Chin. J. Catal.* **2023**, *46*, 48–55. [[CrossRef](#)]
71. Soltani, M.; Amin, H.M.A.; Cebe, A.; Ayata, S.; Baltruschat, H. Metal-Supported Perovskite as an Efficient Bifunctional Electrocatalyst for Oxygen Reduction and Evolution: Substrate Effect. *J. Electrochem. Soc.* **2021**, *168*, 034504. [[CrossRef](#)]
72. Wang, Y.; Cao, L.; Libretto, N.J.; Li, X.; Li, C.; Wan, Y. Ensemble Effect in Bimetallic Electrocatalysts for CO_2 Reduction. *J. Am. Chem. Soc.* **2019**, *141*, 16635–16642. [[CrossRef](#)] [[PubMed](#)]
73. Wu, P.; Liu, H.; Cao, Y.; Xi, S.; Li, Z.; He, Z. Mesostructured cellular foam silica supported Au-Pt nanoalloy: Enrichment of d-state electrons for promoting the catalytic synergy. *Microporous Mesoporous Mater.* **2021**, *316*, 110982. [[CrossRef](#)]
74. Yin, S.; Shen, Y.; Zhang, J.; Yin, H.-M.; Liu, X.-Z.; Ding, Y. Tuning the electronic structure of nanoporous Ag via alloying effect from Cu to boost the ORR and Zn-air battery performance. *Appl. Surf. Sci.* **2021**, *545*, 149042. [[CrossRef](#)]
75. Liu, Y.; Du, L.; Kong, F.; Han, G.; Gao, Y.; Du, C. Sulfur Dioxide-Tolerant Bimetallic PtRu Catalyst toward Oxygen Electroreduction. *ACS Sustain. Chem. Eng.* **2019**, *8*, 1295–1301. [[CrossRef](#)]
76. Zhao, K.; Shu, Y.; Li, F.; Peng, G. Bimetallic catalysts as electrocatalytic cathode materials for the oxygen reduction reaction in microbial fuel cell: A review. *Green Energy Environ.* **2023**, *8*, 1043–1070. [[CrossRef](#)]
77. Karmodak, N.; Norskov, J.K. Activity and Stability of Single- and Di-Atom Catalysts for the O_2 Reduction Reaction. *Angew. Chem. Int. Ed.* **2023**, *22*, e202311113.
78. Guo, D.; Wang, Y.; Lu, P.; Liu, J.; Liu, Y. Flow-through electro-Fenton using nanoconfined Fe-Mn bimetallic oxides: Ionization potential-dependent micropollutants degradation mechanism. *Appl. Catal. B-Environ.* **2023**, *328*, 122538. [[CrossRef](#)]
79. Huang, S.; Qiao, Z.; Sun, P.; Qiao, K.; Pei, K.; Yang, L.; Xu, H.; Wang, S.; Huang, Y.; Yan, Y.; et al. The strain induced synergistic catalysis of FeN_4 and MnN_3 dual-site catalysts for oxygen reduction in proton-/anion-exchange membrane fuel cells. *Appl. Catal. B-Environ.* **2022**, *317*, 721770. [[CrossRef](#)]
80. Jiao, Y.; Deng, L.; Liu, D.; Jiao, Y.; Wang, D.; Chen, J.-F. Process intensification for Fe/Mn-nitrogen-doped carbon-based catalysts toward efficient oxygen reduction reaction of Zn-air battery. *Chem. Eng. Sci.* **2022**, *259*, 117811. [[CrossRef](#)]

81. Li, J.-K.; Wang, F.-F.; Zhang, Y.; Wang, R.; Zhao, S.-N.; Zang, S.-Q. Engineering the electronic structures of hetero-diatomic iron-manganese sites by d-d orbital hybridization for boosting oxygen reduction. *Appl. Catal. B-Environ.* **2023**, *338*, 123090. [[CrossRef](#)]
82. Li, T.; Hu, Y.; Liu, K.; Yin, J.; Li, Y.; Fu, G.; Zhang, Y.; Tang, Y. Hollow yolk-shell nanoboxes assembled by Fe-doped Mn_3O_4 nanosheets for high-efficiency electrocatalytic oxygen reduction in Zn-Air battery. *Chem. Eng. J.* **2022**, *427*, 131992. [[CrossRef](#)]
83. Lin, S.-Y.; Xia, L.-X.; Zhang, L.; Feng, J.-J.; Zhao, Y.; Wang, A.-J. Highly active Fe centered FeM-N-doped carbon (M=Co/Ni/Mn): A general strategy for efficient oxygen conversion in Zn-air battery. *Chem. Eng. J.* **2021**, *424*, 131992. [[CrossRef](#)]
84. Song, S.; Wang, Y.; Tian, P.; Zang, J. One-step complexation and self-template strategy to synthesis bimetal Fe/Mn-N doped interconnected hierarchical porous carbon for enhancing catalytic oxygen reduction reaction. *Int. J. Hydrogen Energy* **2022**, *47*, 24728–24737. [[CrossRef](#)]
85. Wu, D.H.; Huang, H.; Ul Haq, M.; Zhang, L.; Feng, J.J.; Wang, A.J. Lignin-derived iron carbide/Mn, N, S-codoped carbon nanotubes as a high-efficiency catalyst for synergistically enhanced oxygen reduction reaction and rechargeable zinc-air battery. *J. Colloid Interface Sci.* **2023**, *647*, 1–11. [[CrossRef](#)] [[PubMed](#)]
86. Zhang, Y.X.; Zhang, S.; Huang, H.; Liu, X.; Li, B.; Lee, Y.; Wang, X.; Bai, Y.; Sun, M.; Wu, Y.; et al. General Synthesis of a Diatomic Catalyst Library via a Macroyclic Precursor-Mediated Approach. *J. Am. Chem. Soc.* **2023**, *145*, 4819–4827. [[CrossRef](#)] [[PubMed](#)]
87. Zhao, S.; Ma, Z.; Wan, Z.; Li, J.; Wang, X. Noble-Metal-Free FeMn-N-C catalyst for efficient oxygen reduction reaction in both alkaline and acidic media. *J. Colloid Interface Sci.* **2023**, *642*, 800–809. [[CrossRef](#)] [[PubMed](#)]
88. Chen, Z.; Liao, X.; Sun, C.; Zhao, K.; Ye, D.; Li, J.; Wu, G.; Fang, J.; Zhao, H.; Zhang, J. Enhanced performance of atomically dispersed dual-site Fe-Mn electrocatalysts through cascade reaction mechanism. *Appl. Catal. B-Environ.* **2021**, *288*, 120021. [[CrossRef](#)]
89. Wang, N.; Liang, J.; Liu, J.; Cai, Q.; Li, J.; Chen, J.; Huang, T.; Shi, Z. CoFe nanoparticles dispersed in Co/Fe-N-C support with meso- and macroporous structures as the high-performance catalyst boosting the oxygen reduction reaction for Al/Mg-air batteries. *J. Power Sources* **2022**, *517*, 230707. [[CrossRef](#)]
90. Yasin, G.; Ali, S.; Ibraheem, S.; Kumar, A.; Tabish, M.; Mushtaq, M.A.; Ajmal, S.; Arif, M.; Khan, M.A.; Saad, A.; et al. Simultaneously Engineering the Synergistic-Effects and Coordination-Environment of Dual-Single-Atomic Iron/Cobalt-sites as a Bifunctional Oxygen Electrocatalyst for Rechargeable Zinc-Air Batteries. *ACS Catal.* **2023**, *13*, 2313–2325. [[CrossRef](#)]
91. Zhang, Y.; Zhao, M.; Yang, Q.; Lai, M.; Zhang, J.; Liu, C.; Xu, X.; Jia, J. Agarose-gel-based self-limiting synthesis of a bimetal (Fe and Co)-doped composite as a bifunctional catalyst for a zinc-air battery. *J. Colloid Interface Sci.* **2023**, *635*, 186–196. [[CrossRef](#)]
92. Zhu, W.; Pei, Y.; Douglan, J.C.; Zhang, J.; Zhao, H.; Xue, J.; Wang, Q.; Li, R.; Qin, Y.; Yin, Y.; et al. Multi-scale study on bifunctional Co/Fe-N-C cathode catalyst layers with high active site density for the oxygen reduction reaction. *Appl. Catal. B-Environ.* **2021**, *299*, 120656. [[CrossRef](#)]
93. Zhang, L.; Dong, Y.; Li, L.; Wei, L.; Su, J.; Guo, L. Enhanced oxygen reduction activity and stability of double-layer nitrogen-doped carbon catalyst with abundant Fe-Co dual-atom sites. *Nano Energy* **2023**, *117*, 108854. [[CrossRef](#)]
94. Wang, J.; Liu, X.; Liao, T.; Ma, C.; Chen, B.; Li, Y.; Fan, X.; Peng, W. Fe doping induced selenium vacancy on cobalt selenide for enhanced hydrogen peroxides production. *Appl. Catal. B-Environ.* **2024**, *341*, 123344. [[CrossRef](#)]
95. Xiao, Z.; Sun, P.; Qiao, Z.; Qiao, K.; Xu, H.; Wang, S.; Cao, D. Atomically dispersed Fe-Cu dual-site catalysts synergistically boosting oxygen reduction for hydrogen fuel cells. *Chem. Eng. J.* **2022**, *446*, 137112. [[CrossRef](#)]
96. Bu, M.; Liu, Y.; Liao, S.; Liu, W.; Yang, Z.; Jiang, J.; Gao, X.; Yang, Y.; Liu, H. In-site grown carbon nanotubes connecting Fe/Cu-N-C polyhedrons as robust electrocatalysts for Zn-air batteries. *Carbon* **2023**, *214*, 137112. [[CrossRef](#)]
97. Nie, Z.; Zhang, L.; Zhu, Q.; Ke, Z.; Zhou, Y.; Wågberg, T.; Hu, G. Reversed charge transfer induced by nickel in Fe-Ni/Mo₂C@nitrogen-doped carbon nanobox for promoted reversible oxygen electrocatalysis. *J. Energy Chem.* **2024**, *88*, 202–212. [[CrossRef](#)]
98. Tsai, J.-E.; Hong, W.-X.; Pourzolfaghar, H.; Wang, W.-H.; Li, Y.-Y. A Fe-Ni-Zn triple single-atom catalyst for efficient oxygen reduction and oxygen evolution reaction in rechargeable Zn-air batteries. *Chem. Eng. J.* **2023**, *460*, 141868. [[CrossRef](#)]
99. Zhang, L.; Wang, B.; Hu, J.; Huang, X.; Ma, W.; Li, N.; Wagberg, T.; Hu, G. Nickel-induced charge redistribution in Ni-Fe/Fe₃C@nitrogen-doped carbon nanocage as a robust Mott-Schottky bi-functional oxygen catalyst for rechargeable Zn-air battery. *J. Colloid Interface Sci.* **2022**, *625*, 521–531. [[CrossRef](#)]
100. Chen, D.; Li, G.; Chen, X.; Zhang, Q.; Sui, J.; Li, C.; Zhang, Y.; Hu, J.; Yu, J.; Yu, L.; et al. Developing nitrogen and Co/Fe/Ni multi-doped carbon nanotubes as high-performance bifunctional catalyst for rechargeable zinc-air battery. *J. Colloid Interface Sci.* **2021**, *593*, 204–213. [[CrossRef](#)]
101. Wang, Z.; Li, C.; Liu, Y.; Wu, Y.; Zhang, S.; Deng, C. Atomically dispersed Fe-Ni dual sites in heteroatom doped carbon tyres for efficient oxygen electrocatalysis in rechargeable Zn-Air battery. *J. Energy Chem.* **2023**, *83*, 264–274. [[CrossRef](#)]
102. Yao, B.; Yu, Y.; Wang, Z.; Yang, J.; Zhou, Y.; Dionysiou, D.D. Electro-induced activation of persulfate over N-doped porous carbon decorated with Fe/Ni bimets for organic pollutants enhanced degradation: Synergism of electro-activation and catalytic activation. *Chem. Eng. J.* **2023**, *476*, 146769. [[CrossRef](#)]
103. Zhang, X.; Li, Y.; Jiang, M.; Wei, J.; Ding, X.; Zhu, C.; He, H.; Lai, H.; Shi, J. Engineering the coordination environment in atomic Fe/Ni dual-sites for efficient oxygen electrocatalysis in Zn-air and Mg-air batteries. *Chem. Eng. J.* **2021**, *426*, 130758. [[CrossRef](#)]

104. Wang, B.; Tang, J.; Zhang, X.; Hong, M.; Yang, H.; Guo, X.; Xue, S.; Du, C.; Liu, Z.; Chen, J. Nitrogen doped porous carbon polyhedral supported Fe and Ni dual-metal single-atomic catalysts: Template-free and metal ligand-free synthesis with microwave-assistance and d-band center modulating for boosted ORR catalysis in zinc-air batteries. *Chem. Eng. J.* **2022**, *437*, 135295. [[CrossRef](#)]
105. Yang, G.; Zhu, J.; Yuan, P.; Hu, Y.; Qu, G.; Lu, B.A.; Xue, X.; Yin, H.; Cheng, W.; Cheng, J.; et al. Regulating Fe-spin state by atomically dispersed Mn-N in Fe-N-C catalysts with high oxygen reduction activity. *Nat. Commun.* **2021**, *12*, 1734. [[CrossRef](#)] [[PubMed](#)]
106. He, Y.; Yang, X.; Li, Y.; Liu, L.; Guo, S.; Shu, C.; Liu, F.; Liu, Y.; Tan, Q.; Wu, G. Atomically Dispersed Fe-Co Dual Metal Sites as Bifunctional Oxygen Electrocatalysts for Rechargeable and Flexible Zn-Air Batteries. *ACS Catal.* **2022**, *12*, 1216–1227. [[CrossRef](#)]
107. Zheng, F.-Y.; Li, R.; Xi, S.; Ai, F.; Wang, J. Engineering an iron atom-cluster nanostructure towards efficient and durable electrocatalysis. *J. Mater. Chem. A* **2023**, *11*, 8202–8212. [[CrossRef](#)]
108. Bai, J.; Tang, Y.; Lin, C.; Jiang, X.; Zhang, C.; Qin, H.; Zhou, Q.; Xiang, M.; Lian, Y.; Deng, Y. Iron clusters regulate local charge distribution in Fe-N₄ sites to boost oxygen electroreduction. *J. Colloid Interface Sci.* **2023**, *648*, 440–447. [[CrossRef](#)] [[PubMed](#)]
109. Chen, Y.; He, T.; Liu, Q.; Hu, Y.; Gu, H.; Deng, L.; Liu, H.; Liu, Y.; Liu, Y.-N.; Zhang, Y.; et al. Highly durable iron single-atom catalysts for low-temperature zinc-air batteries by electronic regulation of adjacent iron nanoclusters. *Appl. Catal. B-Environ.* **2023**, *323*, 122163. [[CrossRef](#)]
110. Li, J.-C.; Meng, Y.; Zhong, H.; Zhang, L.; Ding, S.; Lyu, Z.; Beckman, S.P.; Hou, P.-X.; Mei, Y.; Cheng, H.-M.; et al. Supramolecular complex derived carbon nanotubes decorated with iron single atoms and nanoclusters as efficient bifunctional oxygen electrocatalysts for rechargeable Zn-air batteries. *Carbon* **2023**, *205*, 302–309. [[CrossRef](#)]
111. Wang, Z.; Zhou, L.; Li, R.; Qu, K.; Wang, L.; Kang, W.; Li, H.; Xiong, S. Electrocatalytic oxygen reduction of COF-derived porous Fe-Nx nanoclusters/carbon catalyst and application for high performance Zn-air battery. *Microporous Mesoporous Mater.* **2022**, *330*, 111609. [[CrossRef](#)]
112. Zhang, Y.; Gao, X.Y.; Wen, Z.; Yang, C.C.; Jiang, Q. Synchronous bi-modulation by nanoclusters and single atoms for high-efficient oxygen reduction electrocatalysis. *Chem. Eng. J.* **2022**, *446*, 111609. [[CrossRef](#)]
113. Tan, F.; Li, W.; Wang, J.; Min, C.; Li, Z.; Zhang, B.; Zheng, X.; Li, L.; Zhang, L.; Zhou, L.; et al. Clarifying the critical roles of iron in boosting oxygen reduction: Single Fe atoms anchored on carbon vacancies as efficient active sites. *Appl. Catal. B-Environ.* **2022**, *305*, 121035. [[CrossRef](#)]
114. Wu, S.; Jiang, S.; Liu, S.-Q.; Tan, X.; Chen, N.; Luo, J.-L.; Mushrif, S.H.; Cadieu, K.; Li, Z. Single Cu-N₄ sites enable atomic Fe clusters with high-performance oxygen reduction reactions. *Energy Environ. Sci.* **2023**, *16*, 3576–3586. [[CrossRef](#)]
115. Qi, C.; Yang, H.; Sun, Z.; Wang, H.; Xu, N.; Zhu, G.; Wang, L.; Jiang, W.; Yu, X.; Li, X.; et al. Modulating Electronic Structures of Iron Clusters through Orbital Rehybridization by Adjacent Single Copper Sites for Efficient Oxygen Reduction. *Angew. Chem. Int. Ed.* **2023**, *62*, e202308344. [[CrossRef](#)] [[PubMed](#)]
116. Dong, Q.; Li, G.; Liu, F.; Ren, J.; Wang, H.; Wang, R. Cu nanoclusters activating ultrafine Fe₃N nanoparticles via the Mott-Schottky effect for rechargeable zinc-air batteries. *Appl. Catal. B-Environ.* **2023**, *326*, 122415. [[CrossRef](#)]
117. Liu, D.; Liu, J.; Wang, L.; Ma, Z.; Xing, J.; Yang, Y.; Xue, B.; Li, F. Enhanced bifunctional electrocatalytic performance of NiFe-layered double hydroxide activated by ultrasonic-assisted loading of Pd nanoclusters. *Int. J. Hydrogen Energy* **2023**, *49*, 152–168. [[CrossRef](#)]
118. Huang, L.; Zhang, L.; Liu, M.; Zhang, Q.; Chen, Z.; Zheng, L.; Cui, Z.; Zhang, Z.; Liao, S. Nitrogen and atomic Fe co-doped hollow carbon nanocages supporting RuPd nanoclusters as extraordinary high-performance nanoreactor-like cathode for lithium–oxygen batteries. *Energy Storage Mater.* **2023**, *61*, 102874. [[CrossRef](#)]
119. Manjunatha, R.; Dong, L.; Zhai, Z.; Wang, J.; Fu, Q.; Yan, W.; Zhang, J. Pd nanocluster-decorated CoFe composite supported on nitrogen carbon nanotubes as a high-performance trifunctional electrocatalyst. *Green Energy Environ.* **2022**, *7*, 933–947. [[CrossRef](#)]
120. Wu, M.; Yang, X.; Cui, X.; Chen, N.; Du, L.; Cherif, M.; Chiang, F.K.; Wen, Y.; Hassanpour, A.; Vidal, F.; et al. Engineering Fe-N₄ Electronic Structure with Adjacent Co-N₂C₂ and Co Nanoclusters on Carbon Nanotubes for Efficient Oxygen Electrocatalysis. *Nano-Micro Lett.* **2023**, *15*, 232. [[CrossRef](#)]
121. Ruan, Q.D.; Zhang, L.; Feng, J.J.; You, L.X.; Wang, Z.G.; Wang, A.J. Three-dimensional self-supporting superstructured double-sided nanoneedles arrays of iron carbide nanoclusters embedded in manganese, nitrogen co-doped carbon for highly efficient oxygen reduction reaction. *J. Colloid Interface Sci.* **2022**, *614*, 655–665. [[CrossRef](#)] [[PubMed](#)]
122. Li, H.; Shu, X.; Tong, P.; Zhang, J.; An, P.; Lv, Z.; Tian, H.; Zhang, J.; Xia, H. Fe-Ni Alloy Nanoclusters Anchored on Carbon Aerogels as High-Efficiency Oxygen Electrocatalysts in Rechargeable Zn-Air Batteries. *Small* **2021**, *17*, e2102002. [[CrossRef](#)] [[PubMed](#)]
123. Meng, H.L.; Lin, S.Y.; Feng, J.J.; Zhang, L.; Wang, A.J. Coordination regulated pyrolysis synthesis of ultrafine FeNi/(FeNi)₉S₈ nanoclusters/nitrogen, sulfur-codoped graphitic carbon nanosheets as efficient bifunctional oxygen electrocatalysts. *J. Colloid Interface Sci.* **2022**, *610*, 573–582. [[CrossRef](#)] [[PubMed](#)]
124. Wan, X.; Liu, Q.; Liu, J.; Liu, S.; Liu, X.; Zheng, L.; Shang, J.; Yu, R.; Shui, J. Iron atom-cluster interactions increase activity and improve durability in Fe-N-C fuel cells. *Nat. Commun.* **2022**, *13*, 2963. [[CrossRef](#)] [[PubMed](#)]
125. Han, A.; Sun, W.; Wan, X.; Cai, D.; Wang, X.; Li, F.; Shui, J.; Wang, D. Construction of Co₄ Atomic Clusters to Enable Fe-N₄ Motifs with Highly Active and Durable Oxygen Reduction Performance. *Angew. Chem. Int. Ed.* **2023**, *62*, e202303185. [[CrossRef](#)] [[PubMed](#)]

126. Wei, X.; Song, S.; Cai, W.; Luo, X.; Jiao, L.; Fang, Q.; Wang, X.; Wu, N.; Luo, Z.; Wang, H.; et al. Tuning the spin state of Fe single atoms by Pd nanoclusters enables robust oxygen reduction with dissociative pathway. *Chem.* **2023**, *9*, 181–197. [[CrossRef](#)]
127. Lu, X.; Yang, P.; Wan, Y.; Zhang, H.; Xu, H.; Xiao, L. Active site engineering toward atomically dispersed M–N–C catalysts for oxygen reduction reaction. *Coord. Chem. Rev.* **2023**, *495*, 215400. [[CrossRef](#)]
128. Liu, F.; Shi, L.; Lin, X.; Yu, D.; Zhang, C.; Xu, R.; Liu, D.; Qiu, J.; Dai, L. Site-density engineering of single-atomic iron catalysts for high-performance proton exchange membrane fuel cells. *Appl. Catal. B-Environ.* **2022**, *302*, 120860. [[CrossRef](#)]
129. Xiao, F.; Wang, Y.; Xu, G.L.; Yang, F.; Zhu, S.; Sun, C.J.; Cui, Y.; Xu, Z.; Zhao, Q.; Jang, J.; et al. Fe-N-C Boosts the Stability of Supported Platinum Nanoparticles for Fuel Cells. *J. Am. Chem. Soc.* **2022**, *144*, 20372–20384. [[CrossRef](#)]
130. Lu, G.; Men, X.; Tang, R.; Wang, Z.; Cui, H.; Zheng, T.; Wang, M.; Yang, H.; Liu, Z. Bionic Fe-N-C catalyst with abundant exposed Fe-N_x sites and enhanced mass transfer properties for efficient oxygen reduction. *J. Colloid Interface Sci.* **2023**, *655*, 90–99. [[CrossRef](#)]
131. Chen, C.; Li, Y.; Huang, A.; Liu, X.; Li, J.; Zhang, Y.; Chen, Z.; Zhuang, Z.; Wu, Y.; Cheong, W.C.; et al. Engineering Molecular Heterostructured Catalyst for Oxygen Reduction Reaction. *J. Am. Chem. Soc.* **2023**, *145*, 21273–21283. [[CrossRef](#)]
132. Chen, C.; Zhou, S.; Xia, J.; Li, L.; Qian, X.; Yin, F.; He, G.; Chen, H. g-C₃N₄ promoted MOF-derived Fe single atoms anchored on N-doped hierarchically porous carbon for high-performance Zn-air batteries. *J. Colloid Interface Sci.* **2024**, *653*, 551–560. [[CrossRef](#)] [[PubMed](#)]
133. Chen, M.; Kong, F.; Yao, H.; Chen, Y.; Meng, G.; Chang, Z.; Chen, C.; Tian, H.; Wang, L.; Cui, X.; et al. Dual metal-organic frameworks-derived Fe-atomic sites bounded to fine Fe/Fe C nanoparticles for enhanced oxygen electroreduction. *Chem. Eng. J.* **2023**, *453*, 139820. [[CrossRef](#)]
134. da Silva Freitas, W.; D'Epifanio, A.; Lo Vecchio, C.; Gatto, I.; Baglio, V.; Ficca, V.C.A.; Placidi, E.; Mecheri, B. Tailoring MOF structure via iron decoration to enhance ORR in alkaline polymer electrolyte membrane fuel cells. *Chem. Eng. J.* **2023**, *465*, 142987. [[CrossRef](#)]
135. Feng, C.; Guo, Y.; Qiao, S.; Xie, Y.; Zhang, L.; Zhang, L.; Wang, W.; Wang, J. 2-Methylimidazole as a nitrogen source assisted synthesis of a nano-rod-shaped Fe/FeN@N-C catalyst with plentiful FeN active sites and enhanced ORR activity. *Appl. Surf. Sci.* **2020**, *533*, 147481. [[CrossRef](#)]
136. Hu, X.; Min, Y.; Ma, L.-L.; Lu, J.-Y.; Li, H.-C.; Liu, W.-J.; Chen, J.-J.; Yu, H.-Q. Iron-nitrogen doped carbon with exclusive presence of Fe_xN active sites as an efficient ORR electrocatalyst for Zn-air battery. *Appl. Catal. B-Environ.* **2020**, *268*, 118405. [[CrossRef](#)]
137. Liu, Y.; Tu, F.; Zhang, Z.; Zhao, Z.; Guo, P.; Shen, L.; Zhang, Y.; Zhao, L.; Shao, G.; Wang, Z. Molecular scissor tailoring hierarchical architecture of ZIF-derived Fe/N/C catalysts for acidic oxygen reduction reaction. *Appl. Catal. B-Environ.* **2023**, *324*, 122209. [[CrossRef](#)]
138. Niu, W.-J.; Yan, Y.-Y.; Li, R.-J.; Zhao, W.-W.; Chen, J.-L.; Liu, M.-J.; Gu, B.; Liu, W.-W.; Chueh, Y.-L. Identifying the impact of Fe nanoparticles encapsulated by nitrogen-doped carbon to Fe single atom sites for boosting oxygen reduction reaction toward Zn-air batteries. *Chem. Eng. J.* **2023**, *456*, 140858. [[CrossRef](#)]
139. Wang, W.; Gong, J.; Long, Q.; Wang, H.; Huang, J.; Dang, W.; Chen, L.; Li, G.; Hou, Z.; Xu, W. Fe-Fe₃N composite nitrogen-doped carbon framework: Multi-dimensional cross-linked structure boosting performance for the oxygen reduction reaction electrocatalysis and zinc-air batteries. *Appl. Surf. Sci.* **2023**, *639*, 158218. [[CrossRef](#)]
140. Zou, Y.; Li, J.; Yu, Y.; Zhang, J.; Fu, Q.; Zhang, L.; Liao, Q.; Zhu, X. Maximizing Fe-N exposure by tuning surface composition via twice acid treatment based on an ultrathin hollow nanocarbon structure for highly efficient oxygen reduction reaction. *Chem. Eng. J.* **2022**, *432*, 134362. [[CrossRef](#)]
141. Wei, S.; Li, L.; Li, A.; Zhang, L.; Hu, H.; Pang, D.; Zhang, Q.; Xiao, H.; Chen, W. Atomic defects engineering on Fe-N₄ sites for boosting oxygen reduction by in-situ ZnO thermal etching strategy. *Chem. Eng. J.* **2023**, *465*, 142820. [[CrossRef](#)]
142. Han, J.; Bao, H.; Wang, J.-Q.; Zheng, L.; Sun, S.; Wang, Z.L.; Sun, C. 3D N-doped ordered mesoporous carbon supported single-atom Fe-N-C catalysts with superior performance for oxygen reduction reaction and zinc-air battery. *Appl. Catal. B-Environ.* **2021**, *280*, 119411. [[CrossRef](#)]
143. Jiang, M.; Wang, F.; Yang, F.; He, H.; Yang, J.; Zhang, W.; Luo, J.; Zhang, J.; Fu, C. Rationalization on high-loading iron and cobalt dual metal single atoms and mechanistic insight into the oxygen reduction reaction. *Nano Energy* **2022**, *93*, 106793. [[CrossRef](#)]
144. Ma, F.X.; Liu, Z.Q.; Zhang, G.; Xiong, Y.X.; Zhang, M.T.; Zheng, L. Isolating Fe Atoms in N-Doped Carbon Hollow Nanorods through a ZIF-Phase-Transition Strategy for Efficient Oxygen Reduction. *Small* **2022**, *18*, e2205033. [[CrossRef](#)] [[PubMed](#)]
145. Chen, Y.; Huang, J.; Chen, Z.; Shi, C.; Yang, H.; Tang, Y. Molecular Engineering toward High-Crystallinity Yet High-Surface-Area Porous Carbon Nanosheets for Enhanced Electrocatalytic Oxygen Reduction. *Adv. Sci.* **2022**, *9*, e2103477. [[CrossRef](#)]
146. Zhuang, Y.; Yang, J.; Meng, L.; Ma, C.; Peng, L.; Chen, D. Polyaniline-derived carbon nanofibers with a high graphitization degree loading ordered PtNi intermetallic nanoparticles for oxygen reduction reaction. *Ind. Chem. Mater.* **2023**, *1*, 458–464. [[CrossRef](#)]
147. Wang, S.; Wang, H.; Huang, C.; Ye, P.; Luo, X.; Ning, J. Trifunctional electrocatalyst of N-doped graphitic carbon nanosheets encapsulated with CoFe alloy nanocrystals: The key roles of bimetal components and high-content graphitic-N. *Appl. Catal. B-Environ.* **2021**, *298*, 120512. [[CrossRef](#)]
148. Li, Y.; Wang, W.; Cheng, M.; Feng, Y.; Han, X.; Qian, Q. Arming Ru with Oxygen-Vacancy-Enriched RuO₂ Sub-Nanometer Skin Activates Superior Bifunctionality for pH-Universal Overall Water Splitting. *Adv. Mater.* **2023**, *35*, e2206351. [[CrossRef](#)]
149. Ye, W.; Chen, S.; Lin, Y.; Yang, L.; Chen, S.; Zheng, X. Precisely Tuning the Number of Fe Atoms in Clusters on N-Doped Carbon toward Acidic Oxygen Reduction Reaction. *Chem.* **2019**, *5*, 2865–2878. [[CrossRef](#)]

150. Zhou, Y.; Yang, W.; Utetiwabo, W.; Lian, Y.M.; Yin, X.; Zhou, L. Revealing of Active Sites and Catalytic Mechanism in N-Coordinated Fe.; Ni Dual-Doped Carbon with Superior Acidic Oxygen Reduction than Single-Atom Catalyst. *J. Phys. Chem. Lett.* **2020**, *11*, 1404–1410. [[CrossRef](#)]
151. Yin, S.H.; Yang, J.; Han, Y.; Li, G.; Wan, L.Y.; Chen, Y.H. Construction of Highly Active Metal-Containing Nanoparticles and FeCo-N₄ Composite Sites for the Acidic Oxygen Reduction Reaction. *Angew. Chem. Int. Ed.* **2020**, *59*, 21976–21979. [[CrossRef](#)] [[PubMed](#)]
152. Wang, Z.; Jin, X.; Zhu, C.; Liu, Y.; Tan, H.; Ku, R. Atomically Dispersed Co₂-N₆ and Fe-N₄ Costructures Boost Oxygen Reduction Reaction in Both Alkaline and Acidic Media. *Adv. Mater.* **2021**, *33*, e2104718. [[CrossRef](#)] [[PubMed](#)]
153. Ding, S.; Barr, J.A.; Shi, Q.; Zeng, Y.; Tieu, P.; Lyu, Z. Engineering Atomic Single Metal-FeN₄Cl Sites with Enhanced Oxygen-Reduction Activity for High-Performance Proton Exchange Membrane Fuel Cells. *ACS Nano* **2022**, *16*, 15165–15174. [[CrossRef](#)] [[PubMed](#)]
154. Song, S.; Wu, M.; Chen, J.; Mo, Z.; Chen, R.; Wang, K. An Fe-N/S-C hybrid electrocatalyst derived from bimetal-organic framework for efficiently electrocatalyzing oxygen reduction reaction in acidic media. *J. Energy Chem.* **2021**, *52*, 291–300. [[CrossRef](#)]
155. Jin, H.; Zhou, H.; He, D.; Wang, Z.; Wu, Q.; Liang, Q. MOF-derived 3D Fe-N-S co-doped carbon matrix/nanotube nanocomposites with advanced oxygen reduction activity and stability in both acidic and alkaline media. *Appl. Catal. B-Environ.* **2019**, *250*, 143–149. [[CrossRef](#)]
156. Chen, J.; Huang, B.; Cao, R.; Li, L.; Tang, X.; Wu, B. Steering Local Electronic Configuration of Fe–N–C-Based Coupling Catalysts via Ligand Engineering for Efficient Oxygen Electroreduction. *Adv. Funct. Mater.* **2022**, *33*, 2209315. [[CrossRef](#)]
157. Xu, C.; Si, Y.; Hu, B.; Xu, X.; Hu, B.; Jiang, Y. Promoting oxygen reduction via crafting bridge-bonded oxygen ligands on a single-atom iron catalyst. *Inorg. Chem. Front.* **2022**, *9*, 3306–3318. [[CrossRef](#)]
158. Guo, X.; Shi, J.; Li, M.; Zhang, J.; Zheng, X.; Liu, Y. Modulating Coordination of Iron Atom Clusters on N, P, S Triply-Doped Hollow Carbon Support towards Enhanced Electrocatalytic Oxygen Reduction. *Angew. Chem. Int. Ed.* **2023**, *62*, e202314124. [[CrossRef](#)]

Disclaimer/Publisher's Note: The statements, opinions and data contained in all publications are solely those of the individual author(s) and contributor(s) and not of MDPI and/or the editor(s). MDPI and/or the editor(s) disclaim responsibility for any injury to people or property resulting from any ideas, methods, instructions or products referred to in the content.